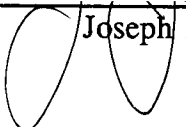


AN ABSTRACT OF THE THESIS OF

Minghua Tian for the degree of Master of Science in Bioresource Engineering Presented on May 31, 1996. Title: Structural Stability Effects on Adsorption of Bacteriophage T4 Lysozyme to Colloidal Silica

Redacted for Privacy

Abstract approved by: _____

 Joseph McGuire

Circular dichroism (CD) spectra were obtained for bacteriophage T4 lysozyme and three of its mutants in the presence and absence of colloidal silica nanoparticles. Mutant lysozymes were produced by substitution of the isoleucine at position 3 with tryptophan, cysteine and leucine. Each substitution resulted in an altered structural stability, quantified by a difference in free energy of unfolding from the wild type. CD spectra recorded in the absence of colloidal silica agreed with x-ray diffraction data in that the mutants and wild type showed similar secondary structures. CD spectra of protein-nanoparticle complexes recorded after contact for 90 minutes showed significant differences from those recorded in the absence of nanoparticles, and these differences varied among the proteins. The percentage of α -helix lost in these proteins upon adsorption to silica nanoparticles was also recorded as a function of time by CD. For a 1:2 protein to particle mixture, different kinetic behaviors were observed among the proteins. The more unstable the protein, the greater the rate and extent of secondary structure loss upon adsorption. For a 1:1 protein to particle mixture, only results recorded with the tryptophan mutant were significantly different from the other variants. The kinetic data recorded for the 1:2 protein to particle ratio was evaluated using two different protein adsorption models. Both models allow proteins at an interface to exist in two different states: state 1 molecules retain their native conformation, while state 2 molecules lose a certain amount of their native secondary structure and occupy more surface area than state 1 molecules. The main difference between these two models is that one allows state 2 molecules to be adsorbed directly from solution, while the other

requires that state 2 molecules be generated by surface-induced conversion of state 1 molecules. The former model showed a better fit to the data than the latter from a least squares comparison. Both models indicated that proteins of lower thermal stability have a greater tendency to adopt state 2 on silica.

Structural Stability Effects on Adsorption of Bacteriophage T4 Lysozyme to Colloidal Silica

by
Minghua Tian

A THESIS

submitted to

Oregon State University

in partial fulfillment of
the requirements for
degree of

Master of Science

Presented May 31, 1996
Commencement June 1997

Master of Science thesis of Minghua Tian presented on May 31, 1996

APPROVED:

Redacted for Privacy

Major Professor, representing Bioresource Engineering

Redacted for Privacy

Head of Department of Bioresource Engineering

Redacted for Privacy

Dean of Graduate School

I understand that my thesis will become part of the permanent collection of Oregon State University libraries. My signature below authorizes release of my thesis to any reader upon request.

Redacted for Privacy

Minghua Tian, Author

ACKNOWLEDGMENT

I would like to thank my major professor, Dr. Joseph McGuire, for his valuable guidance and full support for my two years study here. I also would like to thank my minor professor, Dr. Curtis W. Johnson, for allowing me to use facilities in his lab and providing me valuable instructions. I am grateful to Dr. Thomas K. Plant and Dr. Michelle Bothwell for kindly serving as my committee members.

I would like to thank Dr. Cindy Bower, Woo-Kul Lee, and other fellow graduate students in our lab for their kind help and suggestions. My appreciation is also extended to Jeannie Lawrence, Arazdordi Toumadje, Chartchai Kritinai for their kind help.

Special thanks to Professor Matthews and Sheila Snow of the Institute of Molecular Biology, University of Oregon, for providing bacterial strains needed for this research.

Special thanks to Dr. Adel Faridani for his kind help.

Without the financial support from the Whitaker Foundation, this research could not have been completed.

TABLE OF CONTENTS

	Page
1. INTRODUCTION	1
2. LITERATURE REVIEW	4
2.1 Conformational changes of proteins at interfaces.....	4
2.2 Models used to predict protein behavior at interfaces.....	8
3. MATERIALS AND METHODS	11
3.1 T4 lysozyme and its stability mutants	11
3.2 T4 lysozyme production and purification	14
3.3 Circular dichroism	17
3.4 Solution preparation	19
3.5 Circular dichroism spectra	20
4. RESULTS AND DISCUSSION	23
4.1 CD spectra of proteins in particle-free buffer solution	23
4.2 CD spectra of proteins in the presence of nanoparticles	24
4.3 Analysis according to a two-state, irreversible adsorption model.....	34
4.4 Analysis according to a three-rate-constant adsorption Model.....	55
5. CONCLUSIONS.....	63
BIBLIOGRAPHY.....	64

LIST OF FIGURES

Figure	Page
3.1 The α -carbon backbone of the wild type lysozyme from bacteriophage T4.....	13
3.2 A schematic illustration of a circular dichroism spectrophotometer using modulation method.....	17
4.1 CD spectra of T4 lysozyme and its mutants in phosphate buffer solution.....	24
4.2 CD spectra of protein-nanoparticle complexes after 90 minutes of contact.....	25
4.3 Circular dichroism ($\Delta\epsilon$, $M^{-1}.cm^{-1}/\text{amino-bond}$) at 222 nm recorded for the wild type T4 lysozyme mixed with colloidal silica.....	28
4.4 Circular dichroism ($\Delta\epsilon$, $M^{-1}.cm^{-1}/\text{amino-bond}$) at 222 nm recorded for tryptophan mutant mixed with colloidal silica.....	29
4.5 Circular dichroism ($\Delta\epsilon$, $M^{-1}.cm^{-1}/\text{amino-bond}$) at 222 nm recorded for cysteine mutant mixed with colloidal silica.....	30
4.6 Circular dichroism ($\Delta\epsilon$, $M^{-1}.cm^{-1}/\text{amino-bond}$) at 222 nm recorded for leucine mutant mixed with colloidal silica.....	31
4.7 Comparison of the rates of α -helix loss among the T4 variants upon adsorption onto silica nanoparticles	32
4.8 Comparison of the rates of α -helix loss among the T4 variants upon adsorption onto silica nanoparticles	33
4.9 A simple mechanism for T4 lysozyme adsorption into one of two states defined by fractional surface coverage θ_1 and θ_2	35
4.10 Fractional surface coverage of wild type T4 lysozyme on silica nanoparticles ($\Gamma_{\text{max}} = 3.96 \text{ mg/m}^2$).....	41
4.11 Fractional surface coverage of tryptophan mutant on silica nanoparticles ($\Gamma_{\text{max}} = 3.96 \text{ mg/m}^2$).....	42
4.12 Fractional surface coverage of cysteine mutant on silica nanoparticles ($\Gamma_{\text{max}} = 3.96 \text{ mg/m}^2$).....	43
4.13 Fractional surface coverage of leucine mutant on silica nanoparticles ($\Gamma_{\text{max}} = 3.96 \text{ mg/m}^2$).....	44

LIST OF FIGURES (Continued)

Figure	Page
4.14 Fractional surface coverage of wild type T4 lysozyme on silica nanoparticles ($\Gamma_{\max} = 0.1 \text{ mg}/1.638 \text{ m}^2$).....	46
4.15 Fractional surface coverage of tryptophan mutant on silica nanoparticles ($\Gamma_{\max} = 0.1 \text{ mg}/1.638 \text{ m}^2$).....	47
4.16 Fractional surface coverage of cysteine mutant on silica nanoparticles ($\Gamma_{\max} = 0.1 \text{ mg}/1.638 \text{ m}^2$).....	48
4.17 Fractional surface coverage of leucine mutant on silica nanoparticles ($\Gamma_{\max} = 0.1 \text{ mg}/1.638 \text{ m}^2$).....	49
4.18 Adsorbed mass (total fractional surface coverage) predicted according to the model by using the rate constants in Table 4.3 for wild type T4 lysozyme along with the empirical ellipsometry adsorption kinetic data.....	52
4.19 Adsorbed mass (total fractional surface coverage) predicted according to the model by using the rate constants in Table 4.3 for T4 lysozyme tryptophan mutant along with the empirical ellipsometry adsorption kinetic data.....	53
4.20 Adsorbed mass (total fractional surface coverage) predicted according to the model by using the rate constants in Table 4.3 for T4 lysozyme cysteine mutant along with the empirical ellipsometry adsorption kinetic data.....	54
4.21 A mechanism for T4 lysozyme adsorption into one of two states defined by fractional surface coverage θ_1 and θ_2	55
4.22 Regression according to the three-rate-constant model for ellipsometry and CD data of wild type T4 lysozyme simultaneously.....	59
4.23 Regression according to the three-rate-constant model for ellipsometry and CD data of T4 lysozyme tryptophan mutant simultaneously.....	60
4.24 Regression according to the three-rate-constant model for ellipsometry and CD data of T4 lysozyme cysteine mutant simultaneously.....	61

LIST OF TABLES

Table	Page
3.1 Thermal stabilities of the T4 lysozymes used in this work.....	12
4.1 Percentage of alpha-helix content of T4 lysozymes and its three stability mutants	23
4.2 Estimates for the loss of α -helix attributed to molecules adsorbed in state 2.....	38
4.3 Values of the adsorption rate constants estimated with reference to the mechanism described in Figure 4.9 for CD data ($\Gamma_{\max} = 3.96 \text{ mg/m}^2$).....	40
4.4 Values of the adsorption rate constants estimated with reference to the mechanism described in Figure 4.9 for CD data ($\Gamma_{\max} = 0.1 \text{ mg/1.638 m}^2$).....	45
4.5 Values of adsorption rate constants estimated with reference to figure 4.21.....	58

STRUCTURAL STABILITY EFFECTS ON ADSORPTION OF BACTERIOPHAGE T4 LYSOZYME TO COLLOIDAL SILICA

CHAPTER 1

INTRODUCTION

Protein behavior at interfaces is extremely important in many aspects of biotechnology and medicine. For example, bioseparation and purification of proteins by chromatography and foam fractionation methods involve competitive adsorption of proteins and enzymes at solid-liquid and gas-liquid interfaces (Anand *et al.*, 1995). In medicine, the proper transport and delivery of protein drugs from polymeric microcarriers, and the life time of *in vivo* biosensors are closely related to the protein adsorption process (Haynes and Norde, 1995).

Protein is a very complex material. Although the primary amino acid sequence in a protein can be determined by biochemical methods, the formation of its secondary structure, super-secondary structure, and tertiary structure is much harder to assess. The exact relationship between the sequence of amino acids and the secondary and tertiary structure of a protein is not yet fully understood (Andrade *et al.*, 1985). This makes the study of protein adsorption even more complicated. However, despite these difficulties, the study of proteins at interfaces continues because of its importance in so many areas.

Protein adsorption at interfaces has received a great deal of attention from engineers and scientists. It is generally accepted that the protein adsorption process is affected by several factors. First, the stability of the protein: proteins with low stability will adsorb and spread on the interface more easily (Elwing, 1988 and McGuire *et al.*, 1995). Second, hydrophobic interactions between the proteins and the interface: the more hydrophobic the surface and the protein are, the more adsorption will occur at the interface (Malmsten, 1995). Third, electrostatic interactions between proteins and the hydrophilic interfaces

(Shirahama *et al.*, 1990): substantial differences are observed when the pH and ionic strength of the buffer solution are changed (Ramsden *et al.*, 1994 and Kato *et al.*, 1995). These are only a few of many factors that govern protein adsorption. There are still many aspects have not been cleared yet, such as the conformational rearrangement of adsorbed proteins.

The conformation and orientation of proteins at interfaces has been the subject of continuing interest and investigation for both theoretical and practical reasons (Brash and Horbett, 1995). Many studies confirm that proteins do undergo conformational change and orientational rearrangement, e.g. "side-on" or "end-on" adsorption at an interface. Unfortunately, instruments which can detect these changes are not yet widely available, leaving most studies to provide information on protein adsorption by indirect observation.

Circular dichroism (CD) is a popular method for gaining information about a protein's secondary structure, but there are difficulties in distinguishing orientational rearrangement and conformational changes during adsorption (Smith and Clark, 1992). The introduction of nanoparticles as a solid surface for protein adsorption has made it possible to less ambiguously measure adsorbed protein conformational change using circular dichroism (Kondo and Higashitani, 1991).

There are many factors that govern the adsorption process, and it would be useful to learn the specific influence of individual factors. Comparative studies with genetic variants and site-directed mutants of single proteins have particularly demonstrated the importance of structural stability in protein interfacial behavior (McGuire *et al.*, 1995). In this study, we focused on the influence of structural stability on protein adsorption behavior. Bacteriophage T4 lysozyme and three of its single site mutants, which differed only in thermal stability, were selected to study the effects of structural stability on adsorption to silica nanoparticles using CD.

The goal of this research was to provide direct information on conformational changes undergone by proteins after adsorption, and to measure the effect of structural

stability on adsorption kinetic rate constants using two simple adsorption models. Both models allow proteins at an interface to exist in different conformational states, including native and partially unfolded forms.

CHAPTER 2

LITERATURE REVIEW

2.1. Conformational changes of proteins at interfaces

Numerous studies have been conducted on aspects of protein adsorption, but there are still many factors to consider in this process. To study the different adsorption behaviors at an interface, researchers may change one aspect of the system, such as the pH of the protein solution or the ionic strength of the buffer. Additionally, they may vary the surface properties such as surface charge density or hydrophobicity. By varying a single characteristic of a protein, the resulting effects of changes in features such as thermodynamic stability can be more easily evaluated.

More information on time-dependent changes in the structure of proteins in an adsorbed layer is urgently required (Sadana, 1992) and several techniques have been developed to aid in the acquisition of this information. Ellipsometry is one of the most important tools for studying the kinetics of adsorption, and for measuring adsorption isotherms. Recently McGuire *et al.* (1995) used *in situ* ellipsometry to measure differences in interfacial behavior exhibited by bacteriophage T4 lysozyme and selected stability mutants with respect to their dodecyltrimethylammonium-bromide (DTAB)-mediated elutability at hydrophilic and hydrophobic surfaces. Using a mechanism for adsorption involving parallel, irreversible binding into one of two conformational states, they were able to calculate the ratio of proteins considered more tightly bound, to proteins considered less tightly bound. The resulting ratios were directly related to the thermodynamic stability of the protein. In particular, the DTAB-mediated elutability of each variant at each surface increased as protein stability increased.

Information about conformational changes of proteins at an interface can also be obtained by analyzing Fourier transform infrared (FTIR) spectra. Pitt *et al.* (1989)

monitored human plasma vitronectin adsorption kinetics using FTIR and determined that the adsorbed protein loses its beta-sheet structure. For fibrinogen, it was found that some alpha-helical structures were changed into an unordered conformation and the content of beta-turns was increased (Lu and Park, 1991).

Intrinsic ultra violet total internal reflection fluorescence of the tryptophan residues in a protein permits one to monitor the adsorption and desorption of proteins in single component solutions at solid-liquid interfaces. Andrade *et al.* (1984) compared the fluorescent emission of adsorbed proteins to the proteins in different bulk solutions and concluded that conformational changes occur when human plasma fibronectin adsorbs to either hydrophobic or hydrophilic surfaces. Using the same method, Hlady and Andrade (1988) deduced that conformational change in adsorbed bovine serum albumin (BSA) involved the whole BSA molecule, since tryptophan became exposed to a less polar environment while the binding site polarity was increased. The conformational changes of both BSA and lysozyme upon adsorption onto silica nanoparticles were also observed with this method (Clark *et al.*, 1994). Raman spectroscopy (Aurengo *et al.*, 1982), and fluorescence anisotropy decay (Tan and Martic, 1990), have also provided evidence of conformational changes that occur when protein adsorbs.

Isothermal titration microcalorimetry and differential scanning calorimetry were used by Haynes and Norde (1995) to investigate two proteins, hen egg-white lysozyme (LSZ) and bovine milk α -lactalbumin, which are similar in size, shape, and primary structure, but differ in native-state stabilities, hydrophobicity, and electrical properties. Their results suggest that the steady-state conformations of adsorbed LSZ appear to depend on both a balance between the intramolecular and dehydration forces which stabilize the native-state structure of LSZ, and the strong intermolecular forces between the adsorbed protein and the sorbent surface. They also provided evidence to suggest that the conformational dynamics

of (steady-state) adsorbed LSZ remain fairly limited, but the conformation of the polypeptide backbone of adsorbed α -lactalbumin is dynamic.

There are variety of immunochemical methods that make use of the binding characteristics of antibodies. Elwing *et al.* (1988) studied the adsorption behavior of human complement factor 3 (C3) on both hydrophilic and hydrophobic solid surfaces by using anti-C3 as probes for conformational alteration of adsorbed molecules. Their results support the belief that protein molecules change their conformation to a larger extent on hydrophobic surfaces than on hydrophilic surfaces, since the forces acting between the molecules and the surface are larger on hydrophobic surfaces than on hydrophilic ones.

Numerous experiments have been conducted using circular dichroism. It has become an important tool for evaluating the secondary structure of biopolymers. Soderquist and Walton (1980) observed a difference in the CD spectra of native plasma proteins (albumin, γ -globulin, and fibrinogen) and those desorbed from copolypeptide and silicon surfaces. Using the same method, Norde *et al.* (1986) observed a loss in the secondary structure of human plasma albumin after desorption from both hydrophilic and hydrophobic surfaces. They suggested that the entropy increase from the loss in α -helix content largely compensated for the positive change in adsorption enthalpy. For example, adsorption of a negatively charged protein onto a negatively charged hydrophilic surface would proceed spontaneously by virtue of structural changes in the protein molecule.

The use of circular dichroism can only provide limited information about protein adsorption at an interface, since it can not distinguish between the effects of conformational change and orientational rearrangement. Smith *et al.* (1992) used a stacked quartz system to increase the available surface area for adsorption to gain a better CD signal. They found significant differences between native mellittin solution and mellittins adsorbed on the quartz surface, but they were unable to conclude that these differences were induced by the conformational change of mellittin at the surface.

The introduction of silica nanoparticles as adsorbent surfaces provided a useful approach for studying protein adsorption with CD. Kondo *et al.* (1991) monitored the change in conformation of adsorbed protein directly by letting the protein adsorb onto nanoparticle. The diameter of the nanoparticles (15 nm) did not diffract light in these experiments due to their small size. Using this technique, they found that the secondary structure of an adsorbed protein is different from a protein which has been desorbed. They concluded that the structural adaptability of proteins increased with increasing flexibility of the protein. Also the magnitude of the structural change in flexible proteins increased with increasing affinities of the particles for the proteins. In another study, Kondo and Higashitani (1992) investigated the adsorption behavior of several model proteins, which had a wide range of molecular properties, by varying the pH and ionic strength of the buffer. They were able to explain their results by considering protein-surface interactions, such as electrostatic and hydrophobic interactions and the lateral interaction which occurs between adsorbed protein molecules. Another interesting discovery was made by Norde *et al.* (1992). They found that the extent of changes in the secondary structure increased with decreasing concentration of protein in the solution. They also found a major reduction in the α -helix content of adsorbed, "hard" (low compressibility) protein (LSZ) at low surface coverage, but a smaller change at high surface coverage. For the "soft" (high compressibility) protein (BSA), the percentage of α -helix lost during adsorption was explained by a linear function of the adsorbed amount. That is the extent of these α -helix loss increases with decreasing surface coverage.

All the evidences stated above showed that proteins at interface lose some of their native secondary structure, however, are the changes of the secondary structure contributed by all the proteins at an interface or part of them at an interface, in other words, do proteins at interface exist in multiple states? The answer to this is yes. There is large evidence supporting that multiple states of adsorbed protein exist at a solid/liquid interface. The

studies by Mizutani (1980) showed that enzymes retained part of their activity upon adsorption. This implied that proteins at interface can exist from a native state to a largely denatured state. The fact that IgG desorption from silica and n-pentyl silanized silica occurs at two very different rates also supports the fact that multiple states of proteins exist at an interface (Horbett and Brash, 1987). The different elutabilities of T4 lysozyme and its variants (McGuire *et al.*, 1995) also indicated that multiple states of proteins exist at an interface.

In summary, a large amount of evidence exists demonstrating that proteins undergo a conformational change upon adsorption, and multiple states of proteins ranging from native to largely denatured state exist at interfaces.

2.2. Models used to predict protein behavior at interfaces

It is now generally accepted that proteins exist in different conformations at an interface, however, early models for predicting protein adsorption were based on the Langmuir model for gas adsorption. The Langmuir model was originally developed for adsorption involving small, uncharged particles that are uniform over their surface with regard to their ability to interact with the substrate. Unfortunately, these assumptions do not apply to proteins (Horbett and Brash, 1987). The more recently developed models now incorporate these previously ignored characteristics.

Beissinger and Leonard (1981) developed a model based on the Langmuir-Hinshelwood theory. Their model assumed that the proteins near the surface could adsorb reversibly to a loosely held adsorption state 1. After adsorption, the protein could either desorb or undergo a conformational change to a more tightly held adsorption state 2. Additionally, the protein in state 2 was still able to desorb. They also assumed that adsorption had a nonlinear dependence on the protein concentration in the bulk. The adsorption kinetic data of plasma protein were fitted to the model, and the fits were

reasonably good. Then they extended the model to a binary system with the same set of parameter values, and achieved a reasonably good fit.

Lundstrom (1985) developed a similar model, but assumed that adsorption had a linear dependence on bulk protein concentration. He also assumed that there was a difference in occupied surface area between proteins in state 1 (reversible adsorbed state) and in state 2 (irreversible adsorbed state), and that a loosely bound protein layer develops on the first (state 2 molecules) adsorbed layer. They could explain the surface potential change measurement during ovalbumin adsorption by adding the second layer in their model.

Lundstrom and Elwing (1990) developed a model for the exchange reactions that occur between similar and dissimilar protein molecules at an interface. They incorporated in this model the observation that protein adsorption is often an apparently irreversible phenomenon, i.e., the amount of organic material on the surface stays constant (or decreases very little) when the solution in contact with the surface is depleted of proteins. However, protein molecules may desorb from the surface in the presence of other protein molecules. This suggests that exchange reactions take place at the surface. They considered two types of exchange. The first, self exchange, occurs when a molecule that is adsorbed on the surface is exchanged with a molecule of the same kind from the bulk. The second type of exchange involves a multi-component system where a molecule of one kind is exchanged with one of another kind. Their model allowed proteins to exist on the interface in more than two states, in particular, four were considered in this report. Their model predicted a time dependent compositional change of the adsorbed protein layer, and the occurrence of conformationally changed molecules in the solution. However, this model did not consider that different surface areas may be occupied by molecules in different states.

Krisdhasima *et al.* (1992) adapted Lundstrom's model by accounting for self-exchange with an initial reversible binding step, and allowing for only two states of

adsorbed protein: one reversibly adsorbed and one irreversibly adsorbed. Using this model, they obtained a good fit of β -Lactoglobulin adsorption kinetic data on hydrophobic surfaces. Their results indicated that adsorption on surfaces with greater hydrophobicity reached a plateau faster than adsorption on surfaces of less hydrophobic character.

McGuire *et al.* (1995) used a model for adsorption by parallel irreversible reactions which allowed for proteins to adsorb into state 1 and state 2 (state 2 molecules are more denatured and occupy a greater interfacial area than molecules adsorbed in state 1) directly from solution. They measured the elutability of bacteriophage T4 lysozyme and three of its stability mutants after adsorption for 60 minutes, and determined that the fraction of more tightly bound molecules increased with decreasing protein structural stability.

CHAPTER 3

MATERIALS AND METHODS

3.1. T4 lysozyme and its mutants

T4 lysozyme is a small and well characterized protein with 164 amino acid residues. The molecular weight is 18,700 Daltons (Matthews *et al.*, 1973). The dimensions are approximately $54\text{\AA} \times 28\text{\AA} \times 24\text{\AA}$ (Weaver and Matthews, 1987). T4 lysozyme is a basic molecule with an isoelectric point around pH 9, and an excess of nine positive charges at neutral pH (Sun *et al.*, 1991). More than 150 mutants have been purified and most of them have been crystallized in the same form as the wild type protein (Wozniak *et al.*, 1994).

T4-lysozyme contains two distinct domains. Residues 1 to 60 form the N-terminal domain, which contains two α -helices, and all of the β -sheets of the molecule. Residues 80 to 164 form the C-terminal domain, which contains 7 α -helices and no β -sheets. Residues 159 to 164 appear to form a distorted α -helix (Weaver and Matthews, 1987). The two domains are joined by a long α -helix (from residues 60 to 80) that traverses the length of the molecule (Alber and Matthews, 1987). The wild type molecule contains approximately 60% α -helix of its total secondary structure (Toumadje *et al.*, 1992). Figure 3.1 shows the T4 lysozyme backbone with its α -helices and its β -sheets.

Ile3, located in the middle of the molecule as shown in Fig 3.1, is largely inaccessible to solvent and contributes to the hydrophobic core of the protein (Wozniak *et al.*, 1994). It also helps to link the C- and N- terminal domains. The side chain of Ile3 contacts the side chains of methionine at position 6, leucine at position 7, cysteine at

position 97 and isoleucine at position 100. These residues are buried within the protein interior (Matsumura *et al.*, 1988).

In this work we used mutants in which Ile3 was replaced by cysteine, tryptophan, and leucine. The differences in structural stability among the mutants are given by $\Delta\Delta G^0$: the difference between the free energy of unfolding of the mutant protein and that of the wild type at the melting temperature of the wild type lysozyme. The thermal stabilities of the mutants relative to wild type T4 lysozyme are listed in Table 2.1. For the cysteine mutant, a disulfide bond forms between Cys 3 and unpaired Cys 97 which leads to an increased stability for this mutant (Alber and Matthews, 1987). The substitution with leucine for Ile3 has an increased stability because of an increase in hydrophobic stabilization (Matsumura *et al.*, 1988). The substitution of Ile3 for tryptophan showed a decreased stability, because the substitution caused unfavorable steric interactions and resulted in unsatisfied hydrogen bonds.

All of these mutants differ from wild type only in their stabilities. Their secondary and tertiary structures are the same.

Table 3.1. Thermal stabilities of the T4 lysozymes used in this work (Matsumura *et al.*, 1988).

Variants	$\Delta\Delta G^0$ (kcal/mol)
Trp mutant	-2.8
Wild type	0.0
Leu mutant	0.4
Cys mutant	1.2

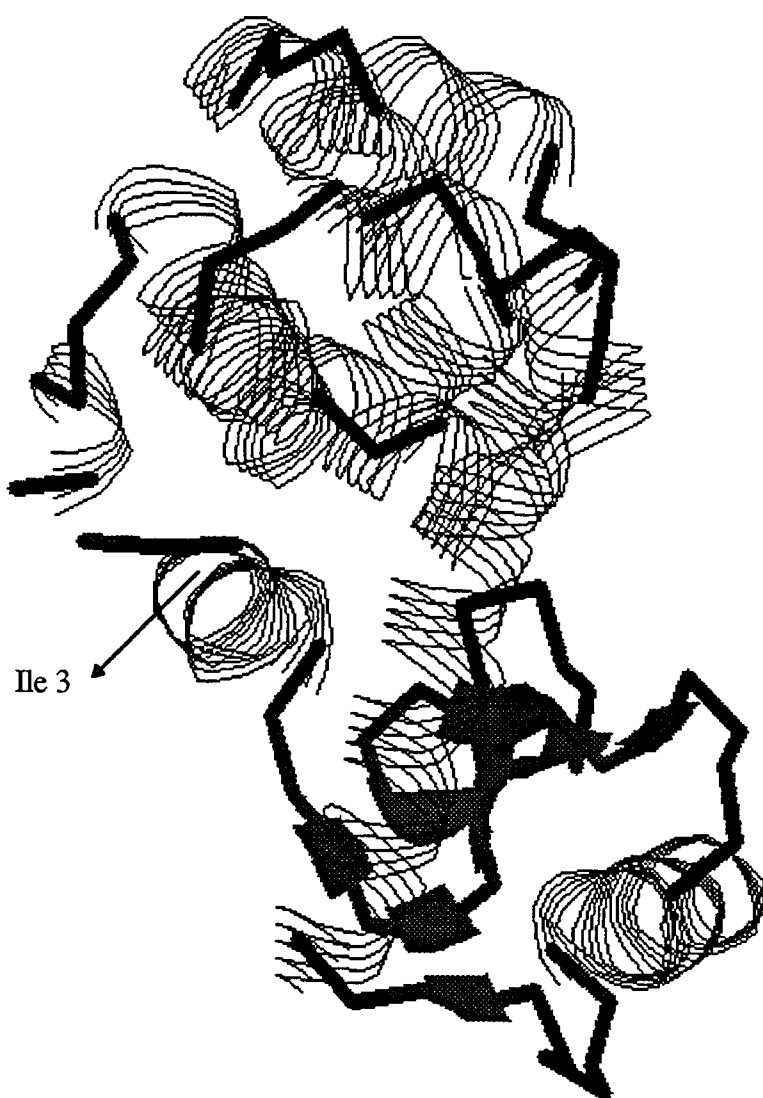


Fig 3.1 The α -carbon backbone of the wild type lysozyme from bacteriophage T4. α -helices and β -sheets are shown as threads and ribbons, respectively.

3.2. T4 lysozyme Production and Purification

Synthetic mutants of T4-lysozyme were produced from transformed cultures of *Escherichia coli* strain RR1. Individual bacteria strains, carrying the mutant lysozyme expression vectors desired for this work, were provided by Professor Brian Matthews and co-workers at the Institute of Molecular Biology, University of Oregon. Expression and purification of T4-lysozyme and its mutants were performed following established procedures (Alber and Matthews, 1987).

3.2.1 Fermentation

Stock cultures of *E. coli* RR1 which carry an ampicillin resistant gene were originally stored in a -80°C freezer. A sterile loop was used to transfer cells bearing the desired mutant lysozyme expression vector to 100 ml LB-H broth (1g tryptone, 0.5g yeast extract, 0.5g NaCl, 0.1 ml 1N NaOH and 100 ml distilled deionized water (DDW)) with 10 mg ampicillin. The cells were allowed to grow at 37°C for 6 to 8 hours before being transferred for fermentation in 4.8 liters of sterilized LB broth (57.6g tryptone, 24 g yeast extract, 48g NaCl, 4.8 g glucose and 4.8 L DDW) with 400 mg ampicillin and 1.5 ml tributyl phosphate (Sigma Chemical Co., St. Louis, MO). The fermenter's temperature (Applikon, Foster City, CA) was kept at 35°C by using a water bath with a circulating system (Model 1120, VWR Scientific, Portland, OR). Agitation was maintained at 600 rpm with a speed controller (ADI 1012, Applikon Dependable Instruments, Schiedam, Holland) while the air flow rate was maintained at 0.8 kg/s. The culture grew under those conditions until its optical density at 595 nm (DU 62 Spectrophotometer, Beckman Instruments, Inc.) was between 0.8 and 1.0 (about 2 hours). Then the temperature of the circulating bath was lowered to 30°C, and the expression of gene which codes for lysozyme production was induced with the addition of 750 mg isopropyl- β -thiogalactoside (IPTG, Sigma Chemical Co., St. Louis, MO) dissolved in 10 ml DDW. The fermentation was allowed to continue

for another 110 minutes at 35°C with an air flow rate of 0.52 kg/s and an agitation of 200 rpm. After this, the desired proteins were ready for harvest.

3.2.2 Centrifugation

The first round of centrifugation was done at 4°C, 13k rpm (JA-14 Rotor, Beckman Model J2-MI Centrifuge, Beckman Instruments Inc., Palo Alto, CA) for 25 minutes. The mutant protein existed in both the supernatant and pellet fraction after the first round of centrifugation. The supernatant was re-centrifuged again at 12.5k rpm for 30 minutes, and this second spin pellet was discarded. The first spin pellets were resuspended with 20 ml of 10 mM Tris buffer at pH 7.4. Following, it was combined with lysis buffer of pH 6.6 (0.1 M sodium phosphate buffer, 0.2 M NaCl, 10 mM MgCl₂) to a final volume of 200 ml, followed by the addition of 1 ml of 0.5 M ethylenediamine tetraacetic acid at pH 8.0 (EDTA, Sigma Chemical Co.) to each 100 ml of resuspended pellet. The mixture was then stirred in the cold room (4°C) for about 12 hours. After that, 0.01 mg of deoxyribonuclease I (Dnase I, crude powder from bovine pancreas, Sigma Chemical Co.) and 1 ml of 1 M MgCl₂ were added to each 100 ml of pellet suspension. This suspension was stirred at room temperature for 2 hours, and then centrifuged at 20k rpm (JA-20 Rotor, Beckman Model J2-MI Centrifuge, Beckman Instruments Inc., Palo Alto, CA) for about 30 minutes. The pellet of this last centrifugation was discarded and the supernatant was combined with that from the original centrifugation.

3.2.3 Purification

About 1100 ml of the supernatant from the centrifugation was dialyzed in 1200 ml plastic fleakers against about 4 liters DDW with Spectra/Por regenerated cellulose hollow fiber bundles (MWCO 18,000, Spectrum Medical Industries, Inc., Houston, TX) until the conductivity (Cond/TDS, Corning Glass Works, Corning, NY) of the supernatant was

between 2 and 3 $\mu\text{mho/cm}$. Then the pH of the solution was adjusted to 6.5-7.5 with 1 N NaOH or 1 N HCl. The whole dialysis process required approximately 48 hours.

The dialyzed solution was then loaded onto a CM Sepharose ion exchange column (CM sepharose CL-6B CCL-100, Sigma Chemical Co.) which was previously equilibrated with 50 mM Tris buffer at pH 7.25. As the dialysate moved through the column, a thick white band of protein could be observed forming on the top of the sepharose. After all the solution had passed through the column, the column was then rinsed with 150 to 200 ml of 50 mM Tris buffer to remove any yellow colored materials which would interfere with the UV signal during elution of the lysozyme. A salt gradient of 50 mM to 0.3 M NaCl in 50 mM Tris buffer was used to elute the protein from the column into a fraction collector (Frac-100, Pharmacia LKB Biotechnology, Alameda, CA). In the meantime, the optical density of the eluant corresponding to the fraction was recorded on a chart recorder. The fractions containing proteins were collected and transferred into Spectra/Por molecular porous membrane tubing (MWCO 12-14K, Spectrum Medical Industries, Inc.) for 12 hours of dialysis against 50 mM sodium phosphate buffer (20 times the eluant volume) of pH 5.8. These procedures were all performed in a cold room at 4°C.

3.2.4 Concentration

The protein solution from the dialysis tubing was concentrated using a SP Sephadex column (SP Sephadex C50, Sigma Chemical CO.). The solution was loaded onto the column, then the lysozyme was eluted from the column with 0.1 M sodium phosphate buffer of pH 6.5. The concentrated solution was stored in 1.5 ml vials without further treatment. The concentration of lysozyme in each vial was determined by measuring the optical density at 280 nm with UV spectrophotometer (Model DU-62, Beckman Instruments, Inc., Fullerton, CA). Samples were diluted 1:100 (1:10 if the protein is not very concentrated in some vials) with 0.1 M sodium phosphate buffer at pH 6.5. Then the

OD was divided by the molar absorption coefficient of 1.28 for wild type and all variants except the tryptophan mutant, which was divided by 1.46 in accordance with Beers law.

3.3. Circular Dichroism

Circular dichroism is an optical phenomena (Figure 3.2) that can be used to evaluate secondary structure of proteins and polypeptides in solution (Johnson, 1990). CD is the difference in the absorption of left and right circularly polarized light. It can be considered to be the absorption spectrum measured with left circularly polarized light minus the

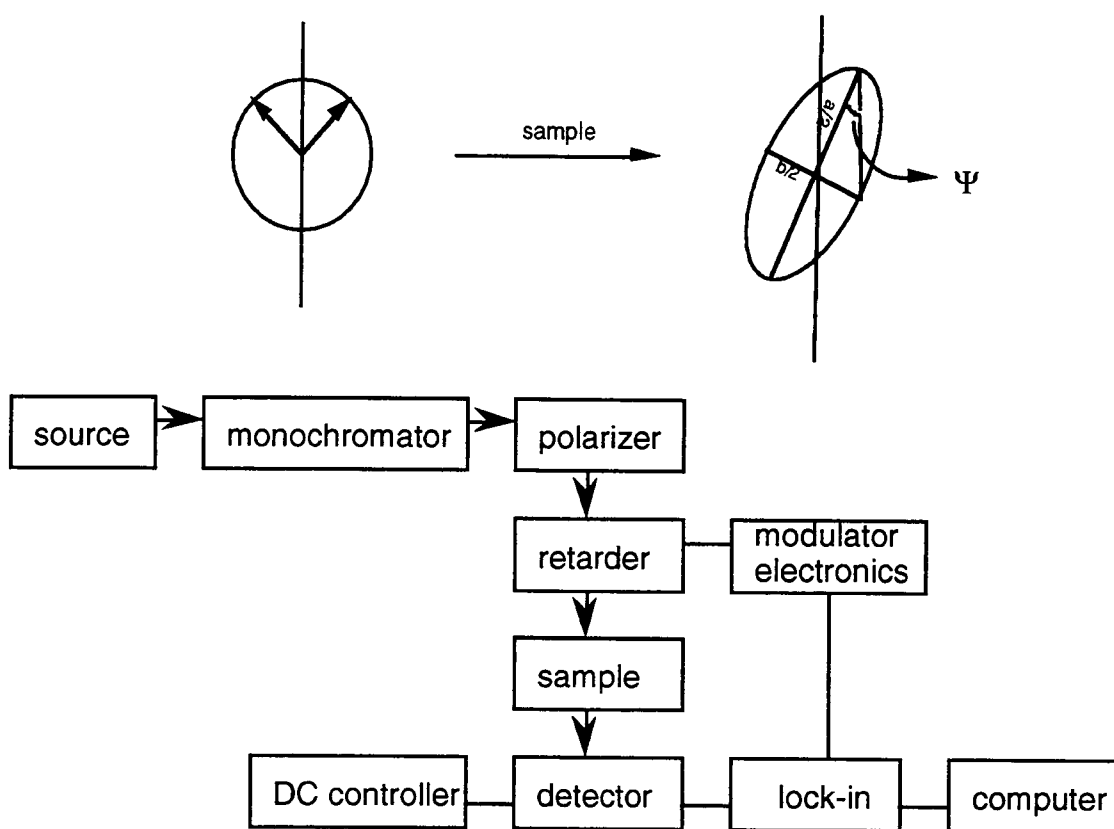


Fig. 3.2 A schematic illustration of a circular dichroism spectrophotometer using modulation method (Johnson, 1996). Also shown are diagrams of the electric vector of light before entering (linear polarized) and after leaving (ellipsoidal shape) an optically active sample. Ψ is the measurement of ellipticity. (Snatzke, 1994)

absorption spectrum measured with right circularly polarized light (Drake, 1994) (Figure 3.2). A solution of randomly oriented molecules will be optically active if the molecules are asymmetric.

The Beer-Lambert law can be used for a quantitative description of circular dichroism:

$$A(\lambda) = \log_{10}(I_0(\lambda)/I(\lambda)) = \epsilon(\lambda)cl \quad [3.1]$$

In equation [3.1], A is the sample absorbance, c is the sample concentration (mol/liter), l is the pathlength (cm) and ϵ is the molar extinction coefficient (molar absorption coefficient, $M^{-1}.cm^{-1}$) which is a constant for each material at a specified wavelength.

From equation [3.1], we can write the differential absorbance:

$$\Delta A(\lambda) = A_L(\lambda) - A_R(\lambda) = (\epsilon_L(\lambda) - \epsilon_R(\lambda))cl = \Delta\epsilon(\lambda)cl \quad [3.2]$$

where A_L and A_R represent the sample absorbance of left and right circularly polarized light respectively.

There exists a simple relationship between difference in absorbance and ellipticity, θ (degrees) from mathematics derivation: (Johnson, 1985)

$$\theta = 32.98 * \Delta A \quad [3.3]$$

The molar ellipticity is an intrinsic quantity, and it can be shown (Johnson, 1985)

$$[\theta] = \frac{100 * \theta * (180/\pi)}{lC} \quad [3.4]$$

where θ is in radians, and molar ellipticity has units of degree·dl·mol⁻¹·dm⁻¹.

From [3.1], [3.2], [3.3], [3.4],

$$\Delta\epsilon = \Delta[\theta] / 3298 \quad [3.5]$$

In this work, the wavelength spectrum is in $\Delta\epsilon$ on a per amide basis; The equation [3.5] was used to compare our data with results measured in terms of ellipticity.

A good approximation of the α -helix content of a protein molecule can be obtained from the CD spectrum ($\Delta\epsilon$) at 222 nm. The absorption band at this wavelength is mainly due to the presence of α -helices, and other secondary structures or chromophores do not have an absorption peak at this wavelength. The relationship between the percentage of α -helix content and $\Delta\epsilon_{222\text{nm}}$ is % α -helix = (-10)* $\Delta\epsilon_{222\text{nm}}$ (Zhong and Johnson, 1992).

3.4. Solution Preparation

3.4.1 Protein Solutions

A pH 7, 0.01M phosphate buffer was used to dilute the stock lysozyme solutions. The buffer was made from Na₂HPO₄ and KH₂PO₄ (Mallinckrodt), both of analytical grade. Distilled deionized water was used in all the solution and suspension preparations of this work. The final concentration of lysozyme, 0.2 mg/ml, was checked by UV-spectrum (Beckman DU-62 Spectrophotometer) at 280 nm.

3.4.2 Nanoparticle Suspensions

Colloidal silica particles (food grade quality) were purchased from EKA-Nobel, Stenumssund, Sweden. The original stock solution contained 5.1×10^{17} particles/ml suspended in pH 10.2 alkaline buffer. The particles were 9 nm in diameter (Billsten *et al.*, 1995), and were used without further modification. The same phosphate buffer used to dilute lysozyme was used to dilute the stock particles. The final concentrations of particles were 3.2×10^{15} particles/ml, 6.4×10^{15} particles/ml, and 12.9×10^{15} particles/ml. The pH of the final dilution was adjusted to between 7 and 7.3 with 1N HCl. These suspensions were prepared in order to supply solid surfaces for protein adsorption, and were used within 6 hours of dilution. Mixing an equal volume of particle suspension and protein solution (0.2 mg/ml) resulted in solutions with protein to particle ratios of 2:1, 1:1, and 1:2 respectively. The light diffraction of the particles in solution is negligible for circular dichroism spectra measurements.

3.5 Circular dichroism spectra

3.5.1 Absorption spectra

The CD instrument can not make accurate measurements on samples with an absorbency (A) greater than 1.0. Thus, it is mandatory to measure the total absorbency of the cuvette, solvent, and sample before attempting to analyze the solution by CD (Johnson, 1990).

Before each CD experiment, the absorption spectrum (Cary 15 spectrophotometer) from 300 to 195 nm was obtained for the buffer, nanoparticle suspensions, lysozyme solution (0.2 mg/ml) and different ratios of protein and nanoparticle solutions (protein to particle ratio is 1:1, 1:2 and 2:1).

3.5.2 Absorption spectra for light scattering

In order to make accurate CD spectra, the light scattering of the sample solution has to be insignificant, so the absorption spectra of the sample solutions were measured from 400 nm to 300 nm.

3.5.3 CSA calibration of the CD instrument

In order to collect accurate CD spectra, the instrument was calibrated by using an aqueous solution of CSA ((+)-10-camphorsulfonic acid) at a concentration of 1 mg/ml in a 1 mm cell. CSA has a CD maximum at 290.5 nm with a $\Delta\epsilon$ of about 2.36 and a CD minimum at 192.5 nm with a $\Delta\epsilon$ of -4.9 (Chen and Yang, 1977). The measurement was made every week at these two wavelength.

3.5.4 Calculation of α -helix content

CD spectra were obtained using the J-720 UV Spectrum (JASCO, Japan). All experiments were carried out at room temperature. The cuvette used in this experiment had a 1 mm pathlength, and was rectangular in shape. It was cleaned after every measurement with 2% RBS-35 detergent for 15 minutes in an ultrasonic cleanser (Branson 1200), then rinsed in water and dried by ethanol. CD spectral data was collected every 0.1 nm, and time scale spectrum data was recorded every 5 seconds with a response time of 1 second and a slide width of 2 nm.

The percentage of α -helix content was calculated using $(-10) \cdot \Delta\epsilon$ (Zhong and Johnson, 1992). The data read from the instrument (ellipticity in millidegrees), were converted to the percentage of alpha-helix using the following equation:

$$\% \alpha - \text{Helix} = \frac{\Delta A_{\text{CSA}} * \theta_{\text{sample}} * \text{MW} * (-10)}{\theta_{\text{CSA}} * c(\text{mg/ml}) * l(\text{cm}) * \text{amino} - \text{bonds/molecule}}$$

where amino-bonds/molecule is the number of amino bonds per protein molecule, and MW is the molecular weight of protein

3.5.5 CD Spectra of T4 lysozymes

Buffer was used to obtain the base line from 260 nm to 195 nm. Then, using the same cuvette, a spectrum in the same range was obtained for T4 lysozyme (0.2 mg/ml).

The net protein spectrum from 260 nm to 195 nm was obtained by subtracting the base line from the protein solution spectrum.

3.5.6 CD spectra of nanoparticle-protein complexes

Nanoparticle-lysozyme solutions were made by transferring 100 μ l of nanoparticle suspension to a clean, dry 10 ml beaker, then transferring the same amount of lysozyme solution into the beaker. The solution was mixed gently for 30 seconds, and then transferred to a cleaned cuvette for immediate analysis by CD. The spectrum at 222 nm was recorded for 90 minutes. A diluted nanoparticle suspension mixed with the same amount of buffer solution was used as a base line for these experiments.

The CD spectra of protein-particle complexes were also recorded from 260 nm to 195 nm, 90 minutes after the nanoparticle and protein were mixed together. The baseline was obtained using the diluted nanoparticle buffer in the same cuvette.

CHAPTER 4

RESULTS AND DISCUSSION**4.1 CD spectra of proteins in particle-free buffer solution**

The CD spectra from 260 to 195 nm for T4 lysozyme and its mutants are plotted in Figure 4.1. These spectra revealed no differences among the variants. This is consistent with the premise that wild type T4 lysozyme and its three mutants differ in stability, but are similar in other aspects. The α -helix content of each protein in buffer solution is shown in Table 4.1. Although the α -helix percentages listed here were calculated from an approximation method, the results are very close to those determined by the CONTIN program (Billsten *et al.*, 1995), which is more accurate and considers the effects of all the secondary structure existing in the molecules. In particular, Billsten *et al.* reported average α -helix contents of 57% for wild type, 58% for cysteine mutant, and 59% for tryptophan mutant. These values are similar to those reported in Table 4.1.

Table 4.1. Percentage of alpha-helix content of T4-lysozyme and its three stability mutants.

protein	Average α -helix content, %	S.D.
Trp mutant	60.3	1.5
Wild type	58.3	0.8
Leu mutant	60.5	2.8
Cys mutant	57.0	0.4

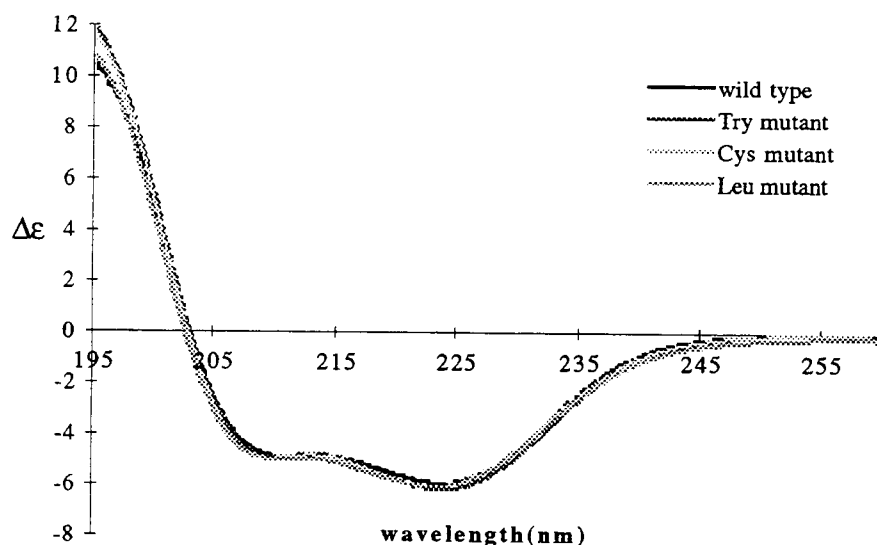


Fig. 4.1. CD spectra of T4 lysozyme and its mutants in phosphate buffer solution

4.2. CD spectra of proteins in the presence of nanoparticles

4.2.1 CD spectra of protein-nanoparticle complexes after 90 minutes

Figure 4.2 shows the CD spectra of wild type T4 lysozyme and its three mutants after being mixed with a nanoparticle suspension for 90 minutes. The intensities of the CD spectra at 222 nm for all variants were reduced after adsorption, implying that the protein had undergone a conformational rearrangement at the silica surface.

4.2.2 Kinetic CD spectra of the complexes

The α -helix content of the T4 lysozyme molecule is about 60%, thus over half of its secondary structure is represented by α -helices. The most appropriate way to calculate the change in secondary structure would be to analyze all components of secondary structure change, including α -helix, β -sheet, β -turn, and random coil. In these experiments, since

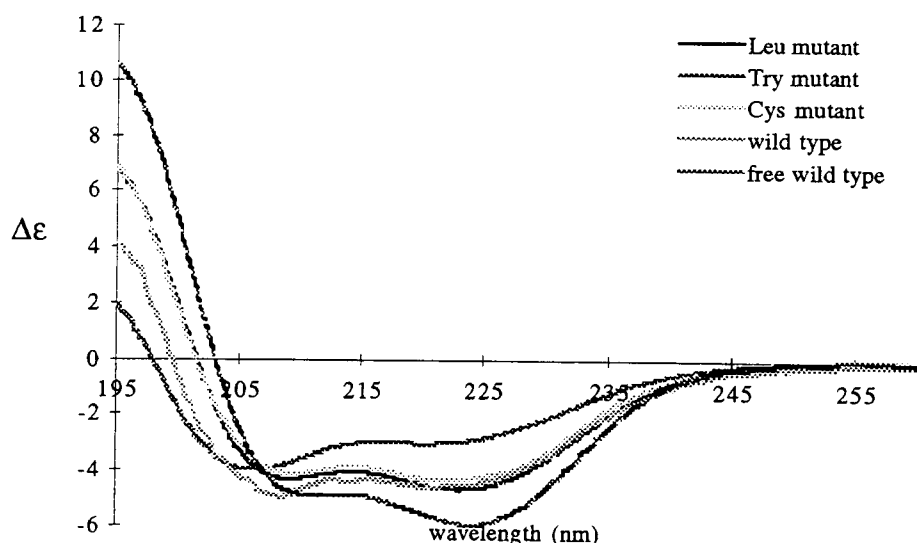


Fig 4.2. CD spectra of protein-nanoparticle complexes after 90 minutes of contact.

the exact value of secondary structure change is not critical for modeling in this work, we chose a simple parameter, α -helix, to represent the approximate "state" of secondary structure. This would be consistent with an assumption that all other secondary structure components denature in similar proportion.

Three different protein to particle ratios (1:1, 1:2 and 2:1) were prepared for each protein. The kinetics of secondary structure changes for two different ratios (1:1 and 1:2) are shown in Figures 4.3-4.6 for each protein. The plots did not include the 2:1 ratio, because when protein was added in excess (2:1), the mixture was unstable and usually denatured within 5 to 30 minutes. From these plots we can see that the first few minutes were similar for the two different ratios. After several minutes the 1:2 mixture started to show a larger change than that of the 1:1 mixture for all the four variants. The reproducibility of experiments recorded with the 1:2 protein to particle mixture was good for all four proteins, but this was not the case with the 1:1 mixture.

The reason for the poor reproducibility of experiments performed with the 1:1 ratio and the instability of the protein-nanoparticle complex at the 2:1 ratio may stem from the colloidal characteristics of the particles. The silica nanoparticles used here were approximately 9 nm in diameter, and were negatively charged in our sample solution of pH 7.0. Nanoparticles in solution are stabilized by an electrostatic repulsion. The collision between particles will occur millions of times per second due to their Brownian motion in the solution (Hunter *et al.*, 1993). The resulting interaction between the proteins adsorbed at a surface will have a profound effect on the stability of the solution (Hunter *et al.*, 1993). At pH 7.0, the T4-lysozyme molecule has 9 out-of-balance positive charges and the adsorption of these molecules on the surface of the nanoparticles changes the net charge of the surface. This decreases the repulsion, thus decreasing the stability of the colloidal suspension. This phenomenon was also observed using the surface force apparatus (Fröberg *et al.*, 1996), where surface repulsion between two negatively-charged mica surfaces disappeared after T4 lysozyme adsorption. For the 2:1 ratio, the number of protein molecules is two times that of the nanoparticles, thus increasing the chances of one particle accommodating more than one protein molecule. This could dramatically change the surface characteristic of the colloids in suspension, and lead to "denaturation" of the protein-particle complex. Denatured protein can be detected visually by the presence of a white, silk-like deposit. It can also be observed by an abrupt change in a CD kinetic curve. In the case of the 1:1 ratio, no denaturation was observed, but reproducibility was poor.

Figures 4.7 and 4.8 show comparisons of the kinetic behavior of the four variants at each protein to particle ratio. The change in secondary structure kinetics exhibited by each stability mutant differed from that of the wild type. The results obtained with the 1:2 mixture were consistent with the results obtained by Billsten *et al.* (1995). The tryptophan mutant displayed the largest and most rapid loss of secondary structure. The most stable mutant, cysteine mutant, lost the smallest amount of secondary structure. The wild type protein and leucine mutant behaved in a manner between these extremes. In other words,

the loss in secondary structure of the more stable variants was lower than that of the less stable mutants. The rate and extent of the secondary structure loss decreased as $\Delta\Delta G$ increased. These results were consistent with previous experiments conducted by McGuire *et al.* (1995), Wang *et al.* (1996), and Fröberg *et al.* (1996). McGuire *et al.* used *in situ* ellipsometry to measure the differences in interfacial behavior exhibited by T4 lysozyme and three of its stability mutants after adsorption for 60 minutes with respect to their dodecyltrimethylammonium bromide (DTAB) -mediated elutability at hydrophilic surfaces. They determined that the fraction of more tightly bound molecules increased with decreasing protein stability. Wang *et al.* used DuNöuy tensiometry to measure the different surface tensions exhibited by T4 lysozyme and four of its stability mutants at the air-water interface, and determined that less stable variants adsorbed in a more tightly bound state. Fröberg *et al.* used the interferometric surface force technique to measure the thicknesses of adsorbed T4 lysozyme films, using wild type and two of its stability mutants. They determined that the thickness of an adsorbed protein layer decreased when the stability of the protein decreased, indicating that less stable variants more easily spread onto the surface.

One would not expect to record much difference between experiments performed with the 1:1 and 1:2 ratios, since in both cases, there was abundant surface area for adsorption, and lateral effects between adsorbed molecules should be small. However, for the 1:1 protein to particle ratio in Figure 4.8, there is not much difference in secondary structure loss among the variants, with the exception of the tryptophan mutant. The difference recorded between the 1:1 ratio and 1:2 ratio might be explained by considering the random movement of the particles in solution. The chance of two molecules adsorbing onto one particle in the 1:1 ratio solution is twice that for the 1:2 ratio. In other words, the protein and particle mixture was possibly not homogeneous, with one protein adsorbed onto one particle, so the lateral effect might be larger for the 1:1 ratio than for the 1:2 ratio.

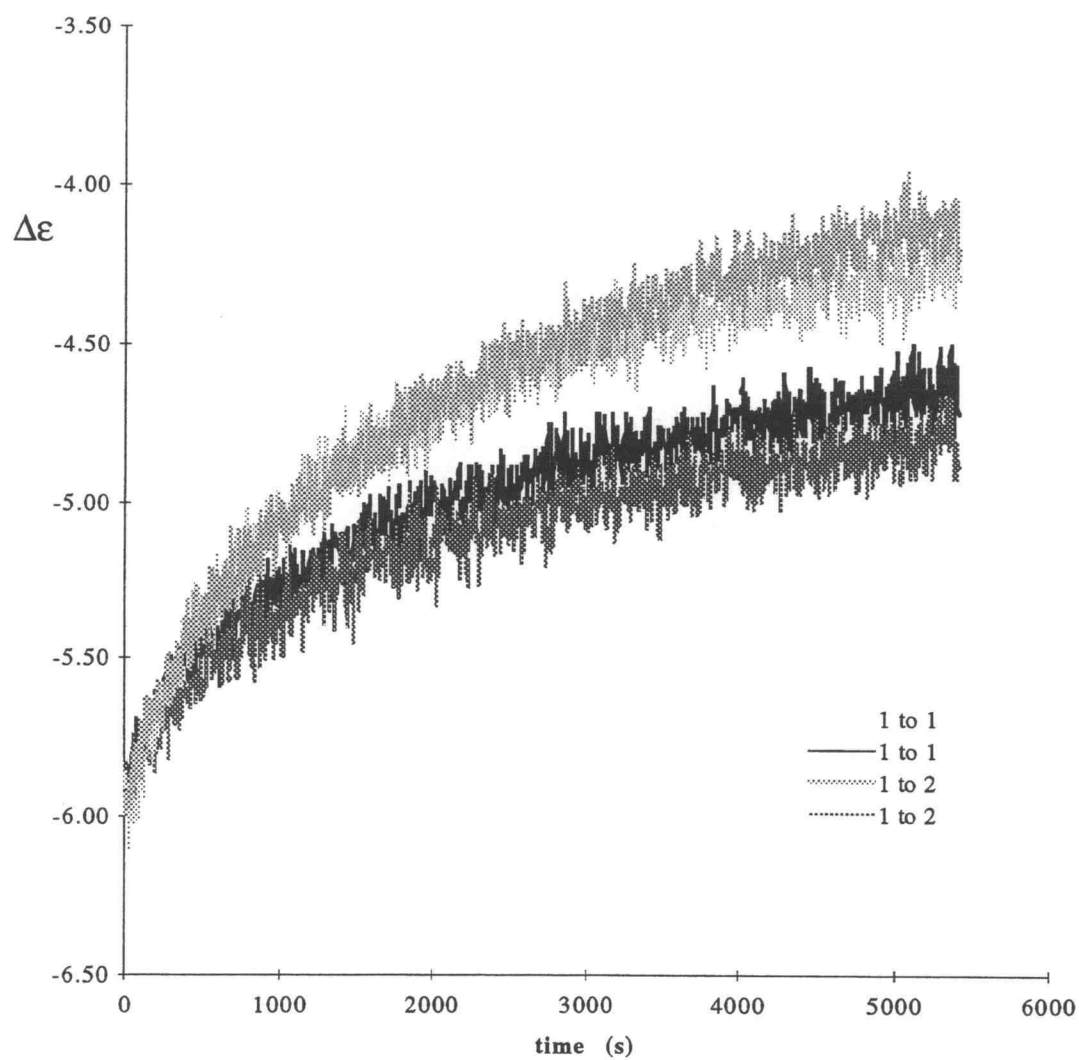


Fig 4.3. Circular dichroism ($\Delta\epsilon$, $M^{-1}.cm^{-1}/\text{amino-bond}$) at 222 nm recorded for the wild type T4 lysozyme mixed with colloidal silica.

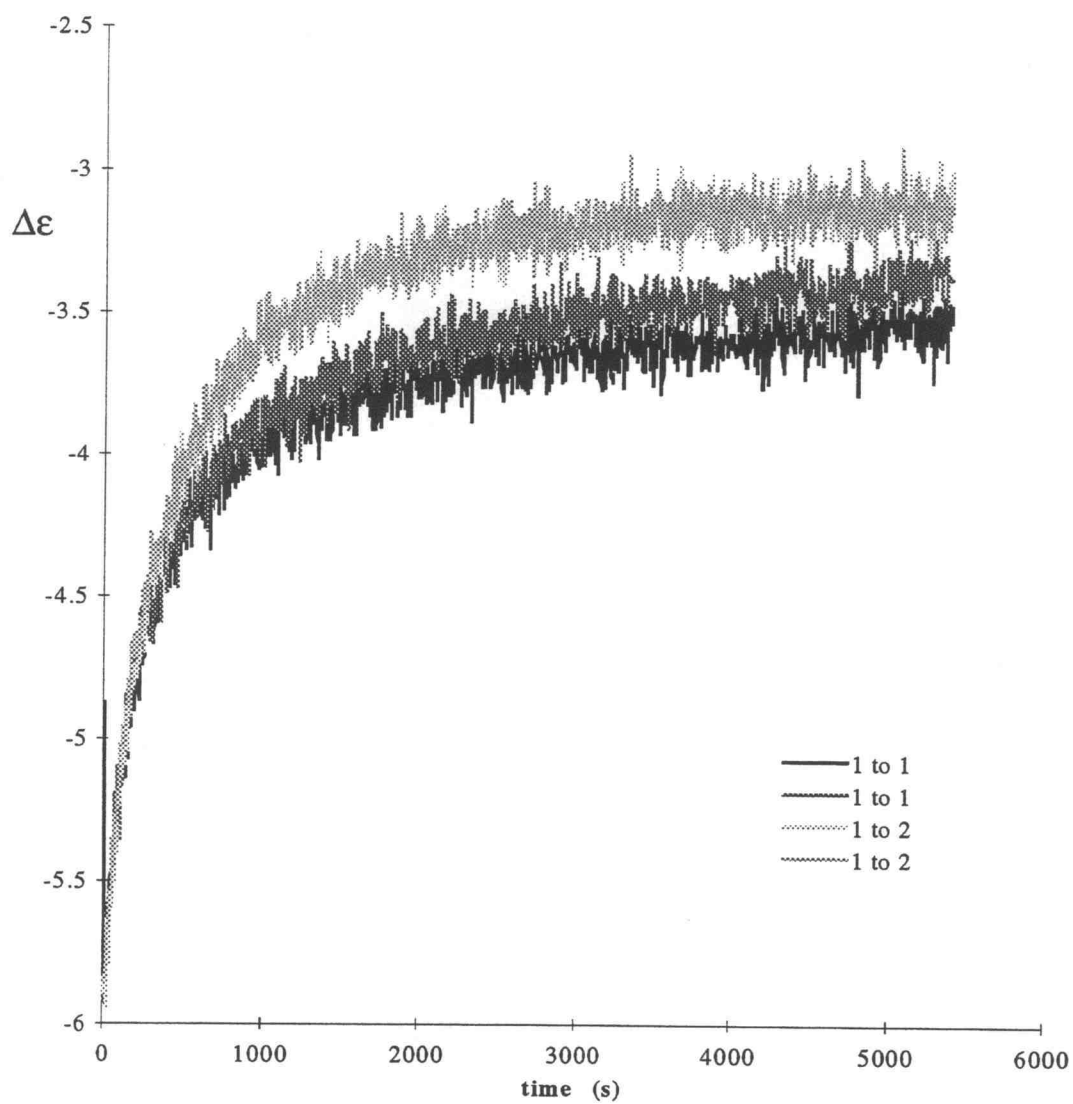


Fig 4.4. Circular dichroism ($\Delta\epsilon$, $M^{-1}.cm^{-1}/\text{amino-bond}$) at 222 nm recorded for the T4 lysozyme tryptophan mutant mixed with colloidal silica.

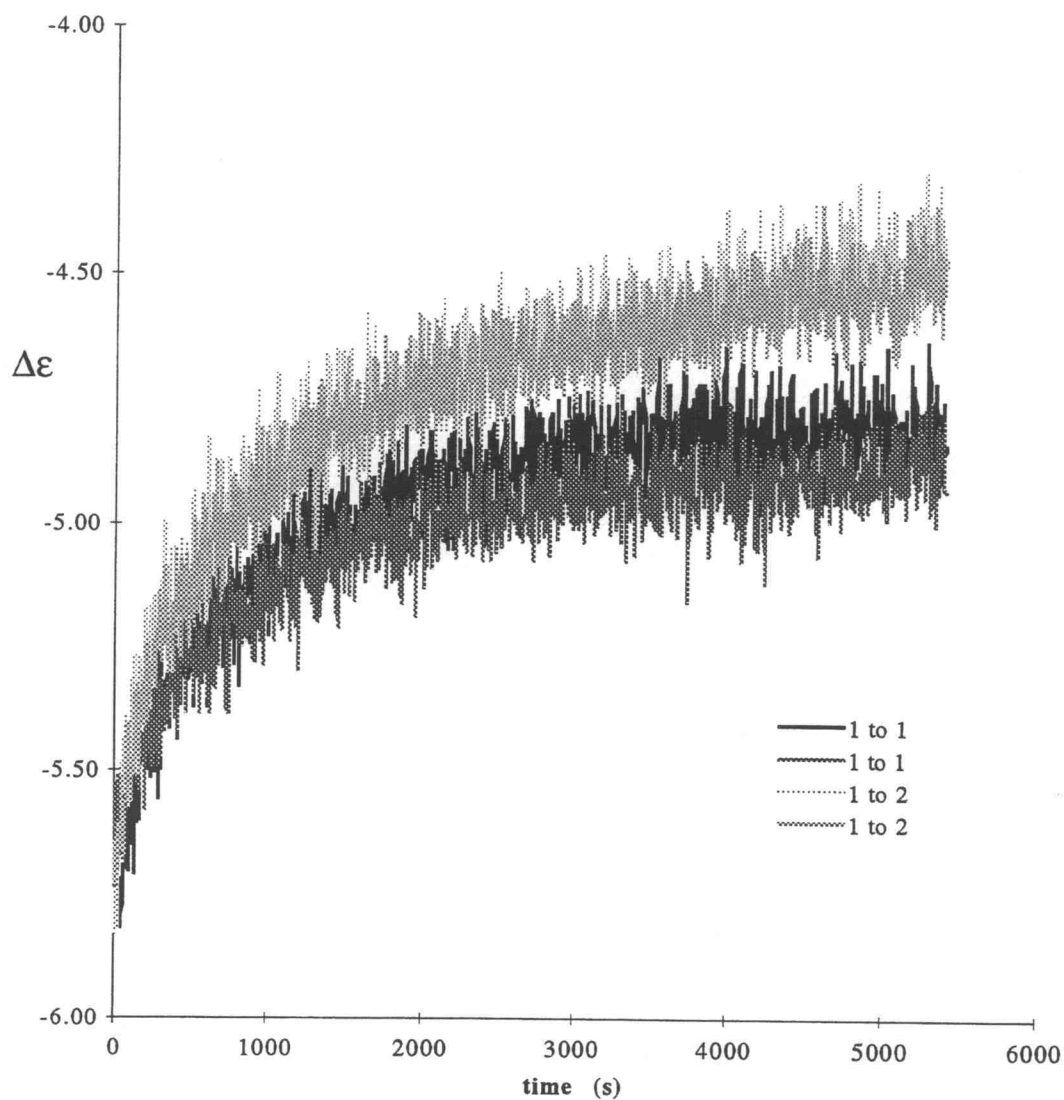


Fig 4.5. Circular dichroism ($\Delta\epsilon$, $M^{-1}.cm^{-1}/amino-bond$) at 222 nm recorded for the T4 lysozyme cysteine mutant mixed with colloidal silica.

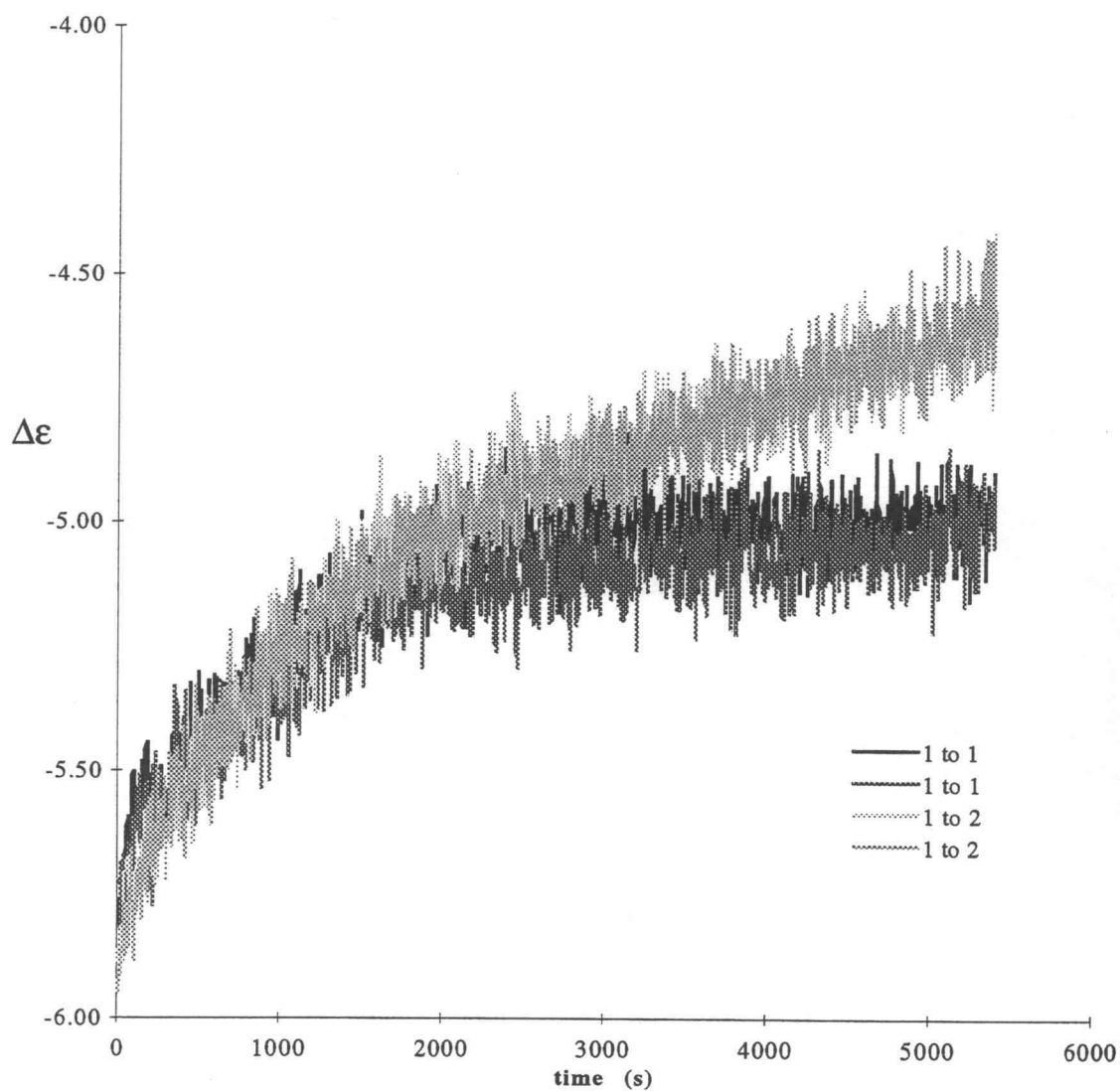


Fig 4.6. Circular dichroism ($\Delta\epsilon$, $M^{-1}\cdot cm^{-1}/\text{amino-bond}$) at 222 nm recorded for the T4 lysozyme leucine mutant mixed with colloidal silica.

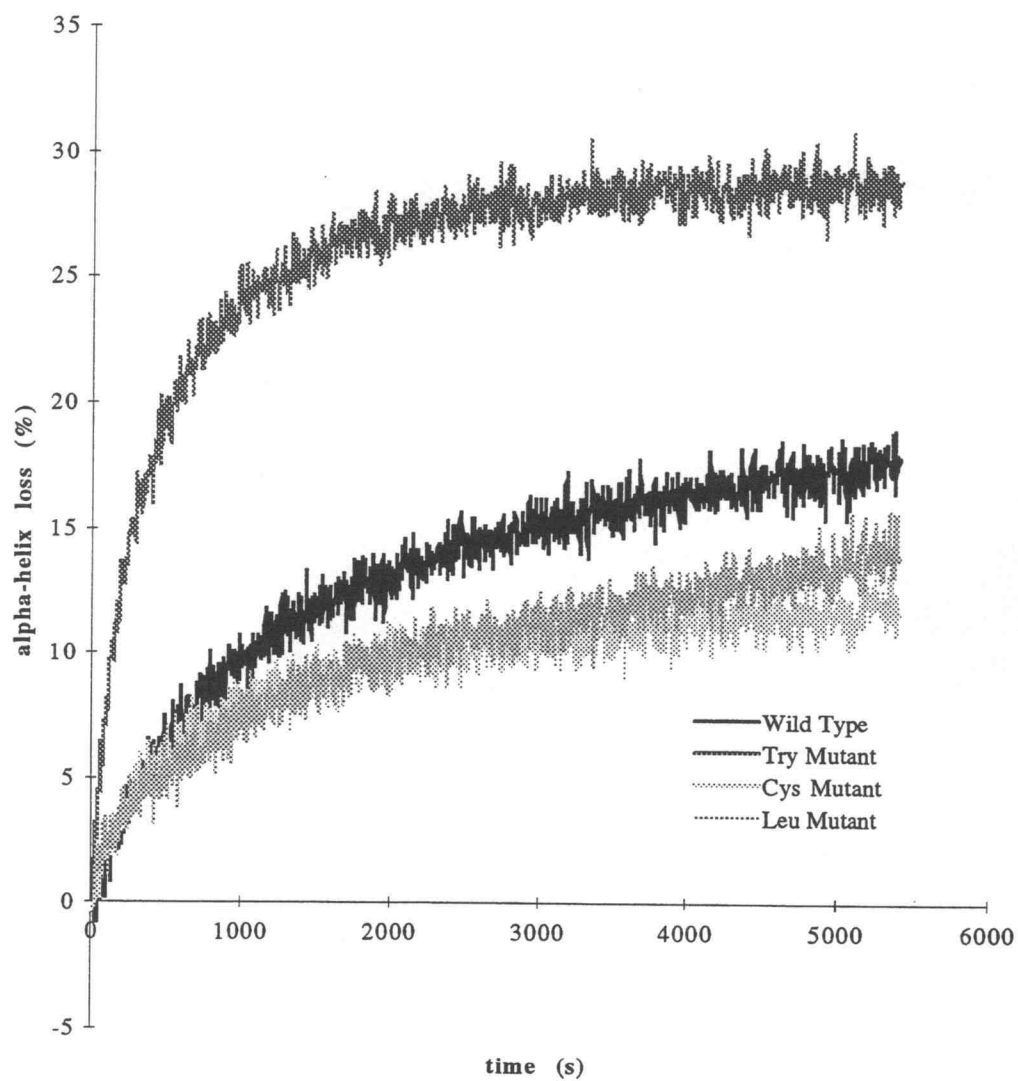


Fig. 4.7. Comparison of the rates of α -helix loss among the T4 variants upon adsorption onto silica nanoparticles. The ratio of protein to particles is 1:2.

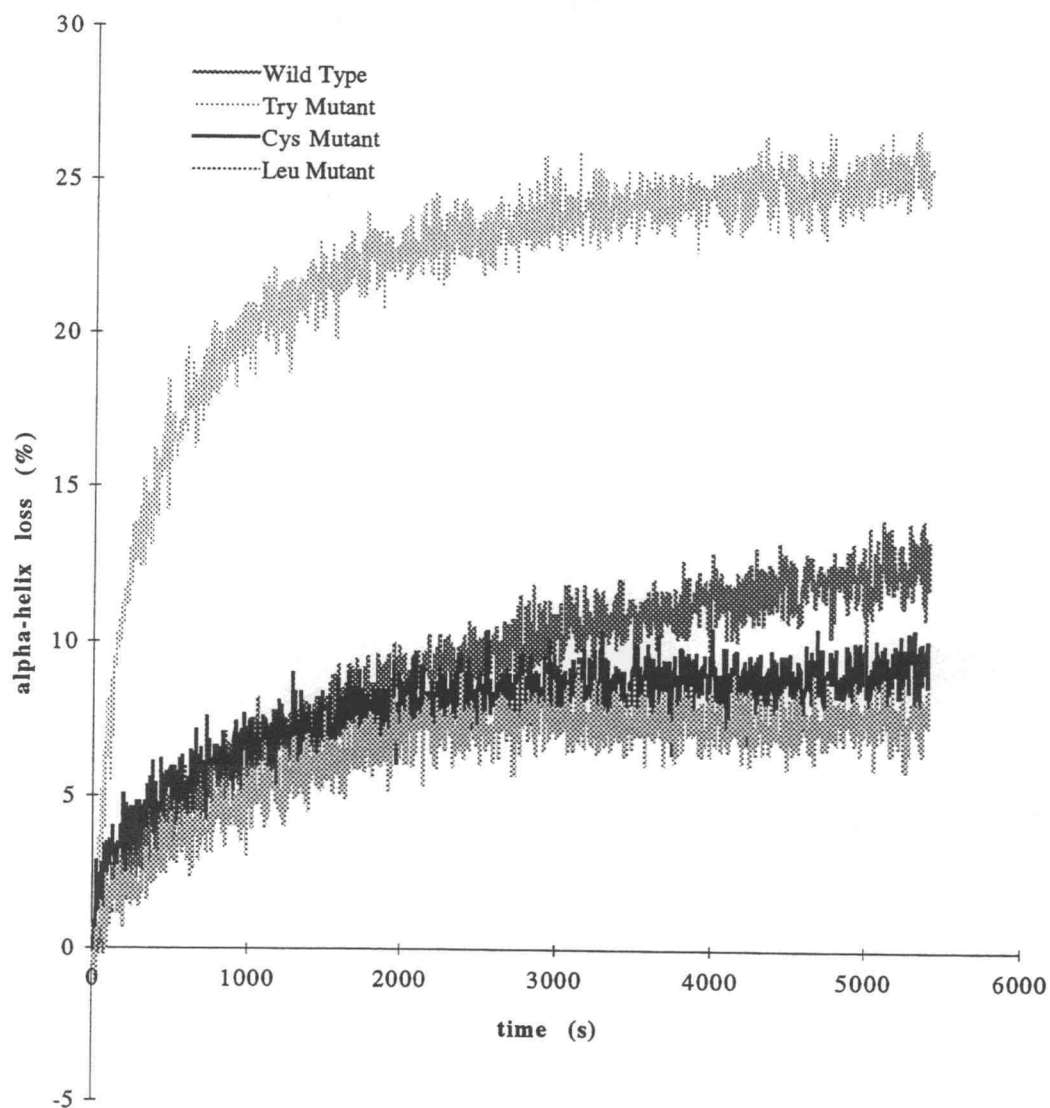


Fig. 4.8. Comparison of the rates of α -helix loss among the T4 variants upon adsorption onto silica nanoparticles. The ratio of protein to particles is 1:1.

Through careful examination of the kinetic curve, some evidence for this is apparent. In the first few minutes there is little difference between the two different ratios. This could be because the adsorbed amount was still low, so the increased available surface area of the 1:2 mixture made no difference. Another possible explanation arises from comparison of these data with a model, described in the next section.

4.3. Analysis according to a two-state irreversible adsorption model

Here we consider that protein molecules from a single-component solution adsorb to the surface of nanoparticles into one of two states as shown in Figure 4.9 with first order adsorption rates constants k_1 for adsorption into state 1 and k_2 for adsorption into state 2. The state 2 molecules are more tightly bound (via more noncovalent contacts) to the surface than those in state 1. Also the state 2 molecules occupy a greater surface area (A_2) than state 1 molecules (A_1). We assume that state 1 molecules retain their secondary structure, but state 2 molecules lose a certain amount of their secondary structure.

In this model, the ratio of the interfacial area occupied by a state 2 molecule to that of a state 1 molecule is denoted as 'a'. From ellipsometry experiment of these proteins (McGuire, 1995), the surface area occupied by a state 2 molecule is approximately equals to that of a side-on adsorbed molecule. The maximum adsorbed mass corresponds to an end on, close packing monolayer. By considering the dimensions of a T4 lysozyme molecule, it is possible to estimate the area necessary for both end-on adsorption (784 \AA^2) and side-on adsorption (1512 \AA^2). These values correspond to an adsorbed mass of 3.96 and 2.05 mg/m² respectively (monolayer), so that the ratio 'a' has a value 1.93.

We denote the fractional surface coverage of state 1 molecules as θ_1 and the fractional surface coverage of state 2 molecules as θ_2 . These values were defined as the adsorbed mass in state 1 or state 2 divided by the maximum adsorbed mass in state 1 (3.96 mg/m²).

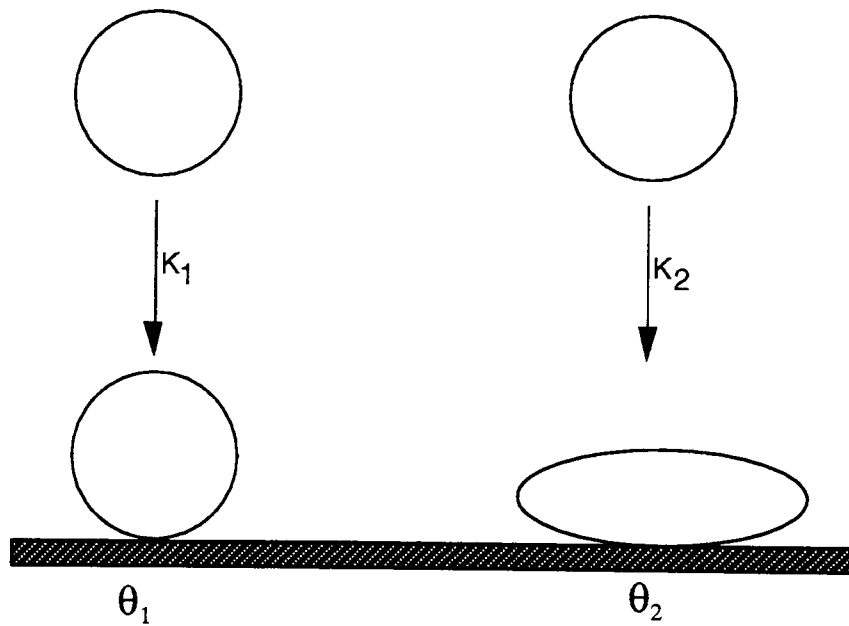


Fig 4.9. A simple mechanism for T4-lysozyme adsorption into one of two states defined by fractional surface coverage θ_1 and θ_2 , where state 2 molecules occupy a greater surface area than molecules adsorbed in state 1 (McGuire *et al.*, 1995).

Equations describing the time-dependent fractional surface coverage of a protein in each of the two states (θ_1 and θ_2) shown in Figure 4.9 can be written as

$$\frac{d\theta_1}{dt} = k_1 * C * (1 - \theta_1 - a * \theta_2) \quad [4.1]$$

and

$$\frac{d\theta_2}{dt} = k_2 * C * (1 - \theta_1 - a * \theta_2) \quad [4.2]$$

where C is the bulk protein concentration (mg/ml). If the concentration of the protein is large compared to the adsorbed amount, we can treat the concentration as a constant during the whole experiment. This is the case in ellipsometry experiments, because of the high concentration of protein solution and small surface area for adsorption. We can solve equations [4.1] and [4.2] directly in that case, yielding

$$\theta_1 = \frac{1}{1 + ak_2/k_1} [1 - \exp(-k_1C - ak_2C)t] \quad [4.3]$$

and

$$\theta_2 = \frac{k_2/k_1}{1 + ak_2/k_1} [1 - \exp(-k_1C - ak_2C)t] \quad [4.4]$$

4.3.1 Interpretation of changes in α -helix content with reference to the model

The CD data provided an estimation of the total percentage of secondary structure loss for all molecules in the sample; however, it is necessary to establish the percentage of secondary structure which is lost for a given state 2 molecule in order to use the mechanism described in Figure 4.9. CD data alone can not provide the answer. However, McGuire *et al.* (1995) used *in situ* ellipsometry to monitor the interfacial behavior of T4 lysozyme and three of its stability mutants. (The same mutants were used in this work, in addition to the leucine mutant). In those experiments, each of the T4 variants was allowed to adsorb onto a hydrophilic silica wafer in a cuvette for 30 minutes (we will refer to this as adsorption kinetic data), and then the silica surface was rinsed with buffer for 5 minutes to remove molecules which were loosely bound. Film properties were monitored for an additional 25

minutes and an apparent decrease in adsorbed mass was observed (this will be referred to as adsorption plateau data). This was followed by addition of DTAB. After 15 minutes the cuvette was rinsed for 5 minutes and the film was again monitored for 25 minutes. With reference to the mechanism described in Figure 4.9, they determined the ratios of state 2 molecules to state 1 molecules present immediately prior to DTAB addition (Table 4.2).

The solid surfaces used in the ellipsometry experiments and in this work were both hydrophilic silica surfaces. Although nanoparticles do not have a perfectly flat surface as is found with the silica wafers, the data can still be reliably compared. The mechanism in Figure 4.9 assumes protein at an interface exists in two states, one that is nearly native, and one that is more denatured. This should not depend on the shape of surface, if the nanoparticle radius of curvature is sufficiently large. Curvature effects in this system are not known, but the volume of a particle is approximately 10 times greater than that of the protein. Additionally, it is generally recognized that the interfacial area of a bound protein is largely independent of the size or molecular weight of the protein (Andrade *et al.*, 1985).

Comparison of CD data with the estimated fractions of each variant adsorbed in state 2 (Table 4.2) enables us to estimate the percentage of α -helix loss consistent with a state 2 molecule. The calculation was based on the following equation:

$$\begin{array}{l} \text{\% } \alpha\text{-helix loss attributed to} \\ \text{a molecule in state 2} \end{array} = \text{Total \% } \alpha\text{-helix loss} * (\theta_1 + \theta_2) / \theta_2$$

These results are shown in Table 4.2. From the data in Table 4.2, it appears that loss of secondary structure estimated for molecules in state 2 generally did not depend on mutant. The secondary structure loss of the cysteine mutant in state 2 is lower than expected, possibly because the ellipsometry data was evaluated with the assumption that the adsorbed mass eventually reaches a monolayer coverage. In actuality, the cysteine mutant may not achieve a full monolayer coverage (McGuire *et al.*, 1995).

The α -helix loss for T4 lysozyme and its mutants in state 2 estimated for the 1:1 ratio was consistently a few percentage points lower than that for the 1:2 ratio. This may be due to adsorption of molecules onto the nanoparticles being incomplete, leaving a fraction of them dissolved in the solution. Additionally, protein-protein interactions on the surface may have led to "incomplete" unfolding.

Table 4.2. Estimates for the loss of α -helix attributed to molecules adsorbed in state 2

protein	$\theta_2/(\theta_1+\theta_2)$ (reference*)	% α -helix loss after 90 min	Protein % α -helix loss attributed to a molecule in state 2
Trp mutant 1:1 ratio	1	24	24
1:2 ratio		29	29
Wild type 1:1 ratio	0.61	12	20
1:2 ratio		18	29
Leu mutant 1:1 ratio			
1:2 ratio			
Cys mutant 1:1 ratio	0.48	10	21
1:2 ratio		12	25

* data from McGuire *et al.* (1995).

Because of this, and the relatively poor reproducibility associated with experiments conducted with the 1:1 mixture, only the data for the 1:2 mixture was analyzed with reference to the adsorption kinetic model evolving from Figure 4.9.

4.3.2. Regression analysis according to the model

The CD data, recorded for the 1:2 mixture, were replotted as fractional surface coverage in state 2 vs. time for each variant, with a state 2 molecule being defined as one having lost 29% α -helix. The conversion was made by the following equation:

$$\% \text{ T4 lysozyme adsorbed in state 2 } (S_2) = [60 - \Delta\epsilon^*(-10)]/x \quad [4.5]$$

where x is the percentage of α -helix loss of a molecule adsorbed at state 2, in this case, $x=29$. We assume that all the nanoparticles used in this work are 9 nm in diameter. The concentration of the nanoparticles is 6.44×10^{15} particles/ml. The total surface area in 1 ml can be calculated as $4 * \pi * (9/2 * 10^{-9})^2 * 6.44 * 10^{15} = 1.638 \text{ m}^2/\text{ml}$. Since the maximum adsorbed mass (Γ_{\max}) for T4-lysozyme is 3.96 mg/m^2 , assuming all proteins adsorb to the nanoparticles,

$$\begin{aligned} \theta_2 &= \frac{\text{adsorbed mass of state 2 molecules (mg/m}^2\text{)}}{3.96 \text{ (mg/m}^2\text{)}} \\ &= S_2 * \frac{0.1 \text{ (mg/ml)}}{1.638 \text{ (m}^2/\text{ml)}} * \frac{1}{3.96 \text{ (mg/m}^2\text{)}} \end{aligned} \quad [4.6]$$

For this experiment, we cannot neglect the change in free protein concentration, thus we can write an equation for the relationship between protein concentration C and θ_1 and θ_2 according to mass balance.

$$dC(\text{mg/ml}) * (1 \text{ ml}) = - (d\theta_1 + d\theta_2) * 1.638 \text{ (m}^2\text{)} * 3.96 \text{ (mg/m}^2\text{)} \quad [4.7]$$

From equation [4.7],

$$\frac{dC}{dt} = - \left(\frac{d\theta_1}{dt} + \frac{d\theta_2}{dt} \right) * 6.49 \quad [4.8]$$

The combination of equations [4.1], [4.2] and [4.8] do not have an analytical solution, however, it was possible to fit the data numerically to estimate k_1 and k_2 in each case. These results are plotted in Figures 4.10-4.13 and the rate constants are tabulated in Table 4.3.

From the plots, it is apparent that the model fits the data well. As expected, k_2 and k_2/k_1 increase as the free energy of unfolding, ΔG^0 , decreases. From equations [4.1] and [4.2], we know that $k_2/k_1 = \theta_2/\theta_1$ at any time. A decrease in the value of k_2/k_1 would indicate that less protein is adopting a state 2 conformation, thus the tendency of the protein to adopt state 2 is increased with a decrease in its stability. This trend is also consistent with those observed in regard to surface tension kinetics of these proteins at the air/water interface (Wang *et al.*, 1995), their surfactant-mediated elutability (McGuire *et al.*, 1995) and surface force measurements (Fröberg *et al.*, 1996). That is less stable mutants tend to adsorb in a more denatured state at an interface, and spread more on the surface. Those mutants would be more resistance to DTAB, and tend to decrease more of the surface tension at the air-water interface.

Table 4.3. Values of the adsorption rate constants estimated with reference to the mechanism described in Figure 4.9 for CD data. ($\Gamma_{\max} = 3.96 \text{ mg/m}^2$)

protein	$k_1(\times 10^{-3})$ (ml/mg·min)	$k_2(\times 10^{-3})$ (ml/mg·min)	k_2/k_1
Trp mutant	0.6	21.2	35.3
Wild type	2.9	4.2	1.5
Leu mutant	11.0	8.0	0.7
Cys mutant	6.3	3.6	0.6

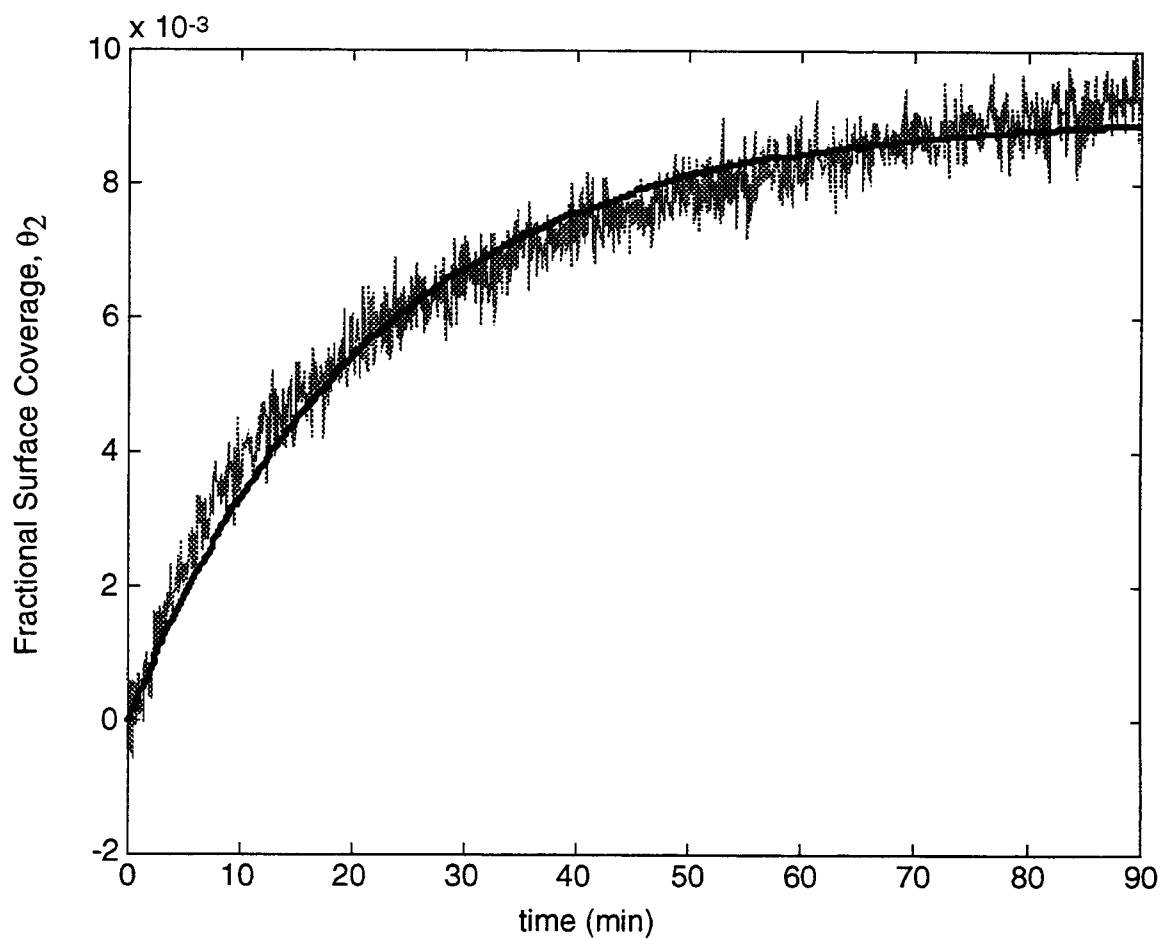


Fig. 4.10. Fractional surface coverage of wild type T4 lysozyme on silica nanoparticles (1:2 mixture). The smooth line is the regressed fit of $\theta_2=f(t)$. ($\Gamma_{\max} = 3.96 \text{ mg/m}^2$)

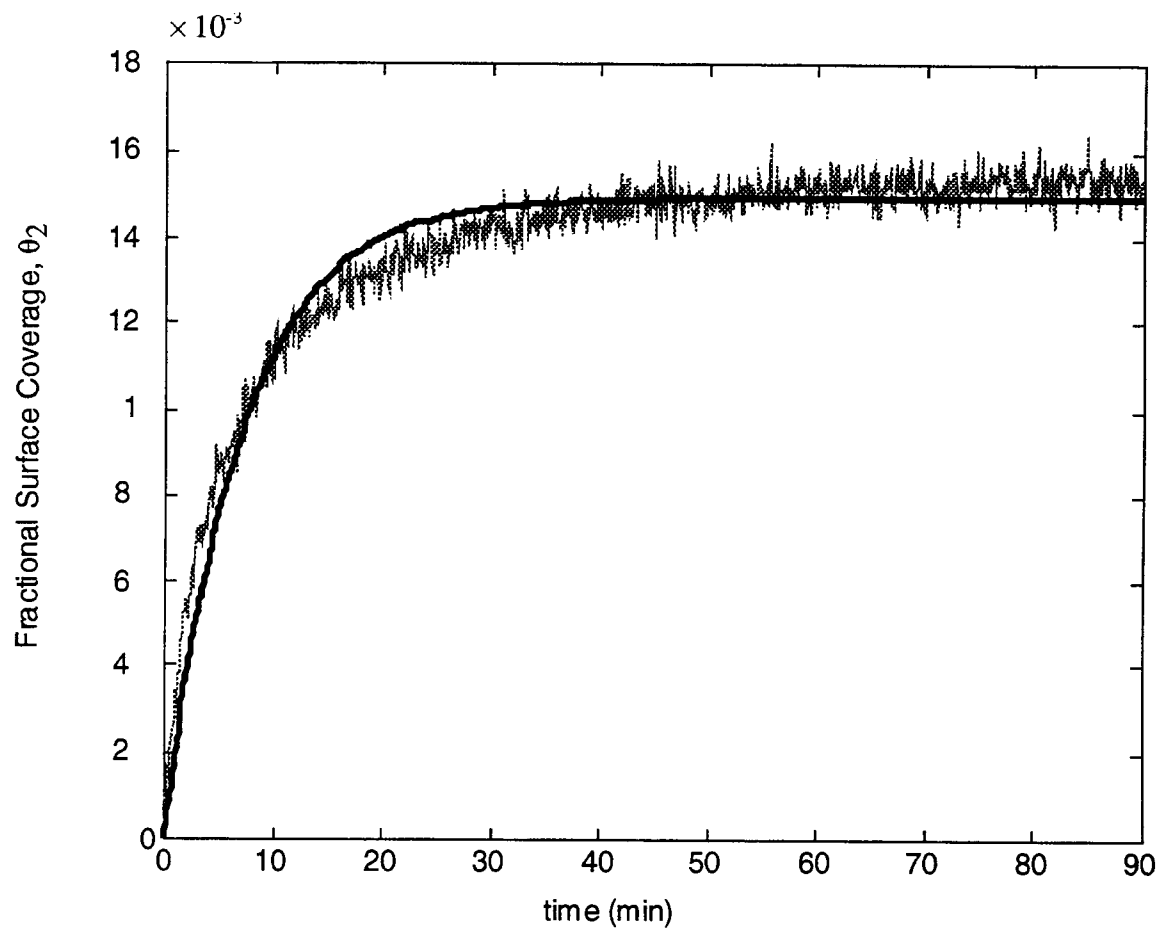


Fig. 4.11. Fractional surface coverage of tryptophan mutant on silica nanoparticles (1:2 mixture). The smooth line is the regressed fit of $\theta_2=f(t)$. ($\Gamma_{\max} = 3.96 \text{ mg/m}^2$)

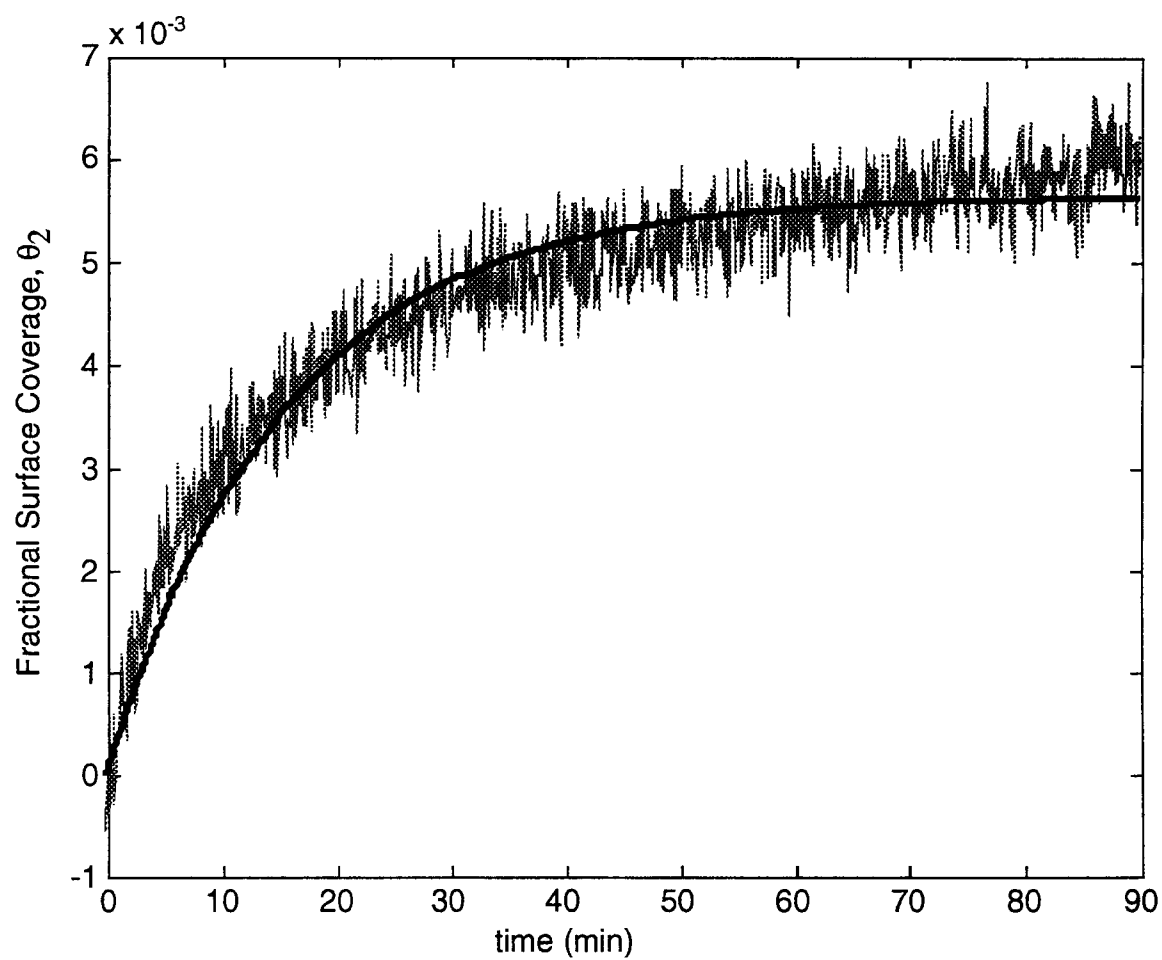


Fig. 4.12. Fractional surface coverage of cysteine mutant on silica nanoparticles (1:2 mixture). The smooth line is the regressed fit of $\theta_2=f(t)$. ($\Gamma_{\max} = 3.96 \text{ mg/m}^2$)

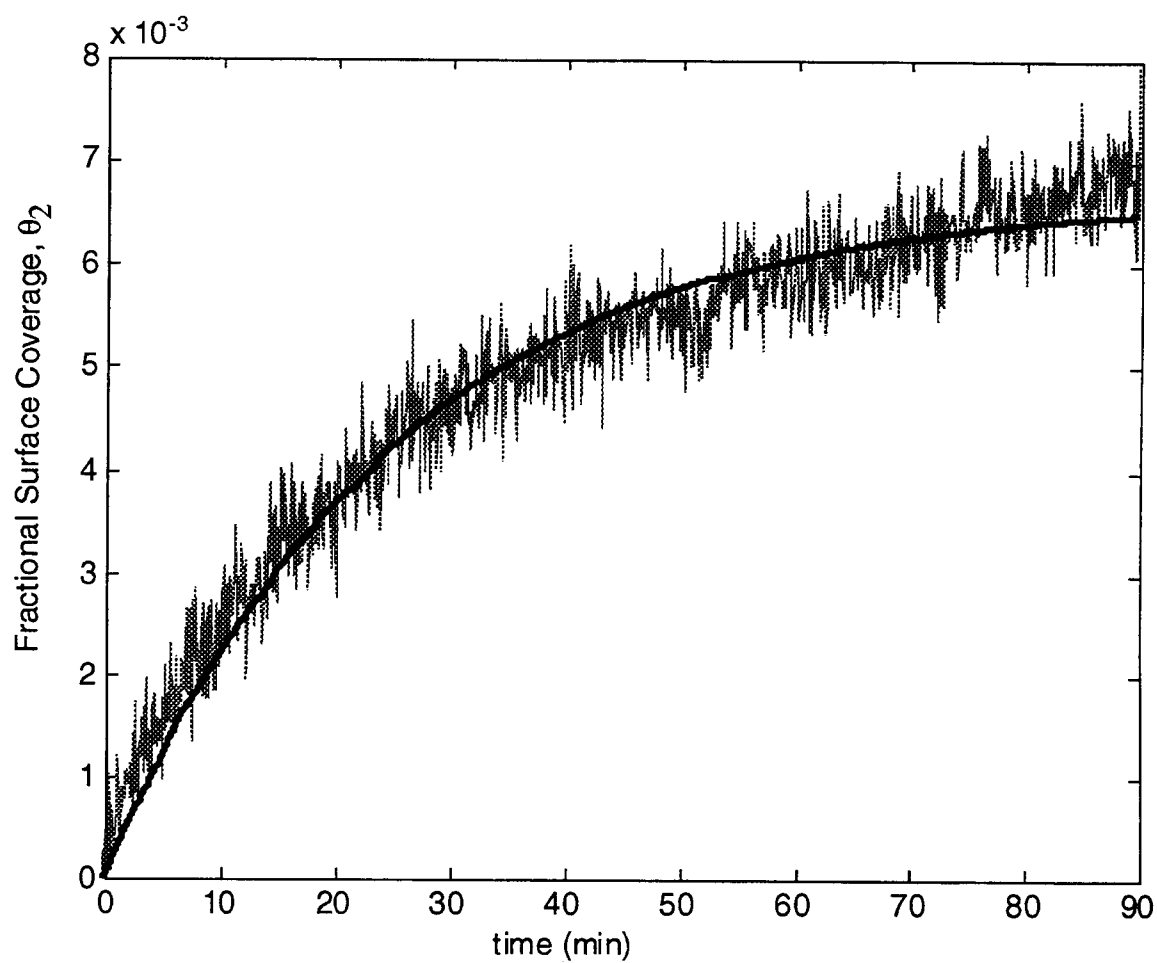


Fig. 4.13. Fractional surface coverage of leucine mutant on silica nanoparticles (1:2 mixture). The smooth line is the regressed fit of $\theta_2=f(t)$. ($\Gamma_{\max} = 3.96 \text{ mg/m}^2$)

4.3.3. Comparison to ellipsometry data with reference to Figure 4.9

As stated before, the solid surface area used for adsorption in the ellipsometry experiment was about one ten-thousandth of that in CD experiment, but the concentration used was ten times higher than CD experiment. In order to compare the ellipsometry data with the CD data, we need to change the definition of θ_1 and θ_2 from the definition we used in equation 4.6 (this definition was used when analysing ellipsometry data according to this model). The maximum obtainable surface coverage is $0.1 \text{ mg}/1.638 \text{ m}^2$, we will use this as the maximum adsorbed amount instead of $3.96 \text{ mg}/\text{m}^2$ when we calculate the θ_1 and θ_2 , thus the equation 4.6 will be simplified as $\theta_2 = S_2$, and the equation 4.8 will be

$$\frac{dC}{dt} = -\left(\frac{d\theta_1}{dt} + \frac{d\theta_2}{dt}\right) * 0.1 \quad [4.9]$$

With the combinations of equations [4.1], [4.2] and [4.9], redo the regression for the CD data. The results are plotted in Figures 4.14-4.17 and the rate constants are tabulated in Table 4.4.

Table 4.4. Values of the adsorption rate constants estimated with reference to the mechanism described in Figure 4.9 for CD data. ($\Gamma_{\max} = 0.1 \text{ mg}/1.638 \text{ m}^2$)

protein	k_1 (ml/mg·min)	k_2 (ml/mg·min)	k_2/k_1
Trp mutant	0.105	0.900	8.56
Wild type	0.195	0.170	0.87
Leu mutant	0.171	0.081	0.48
Cys mutant	0.579	0.231	0.40

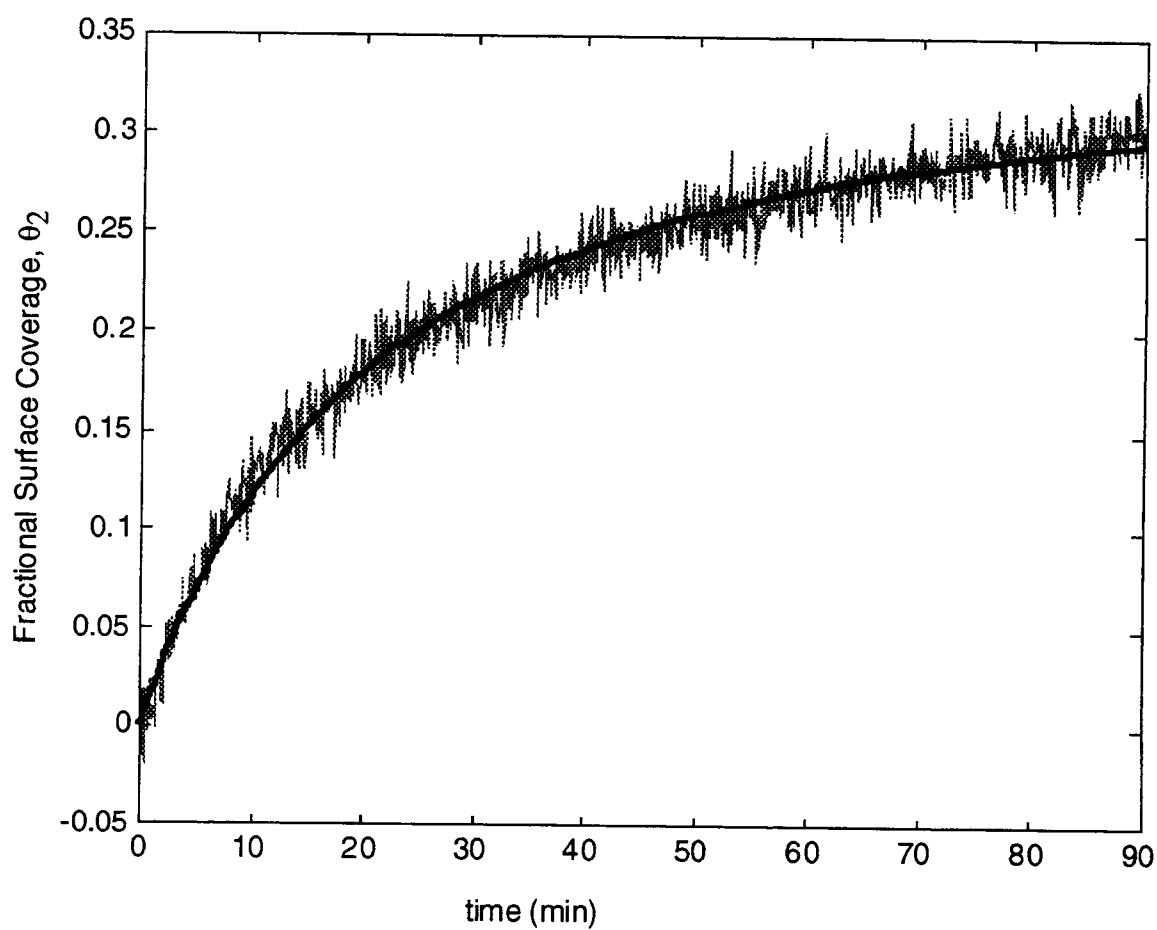


Fig. 4.14. Fractional surface coverage of wild type T4 lysozyme on silica nanoparticles (1:2 mixture). The smooth line is the regressed fit of $\theta_2=f(t)$. ($\Gamma_{\max} = 0.1 \text{ mg}/1.638 \text{ m}^2$)

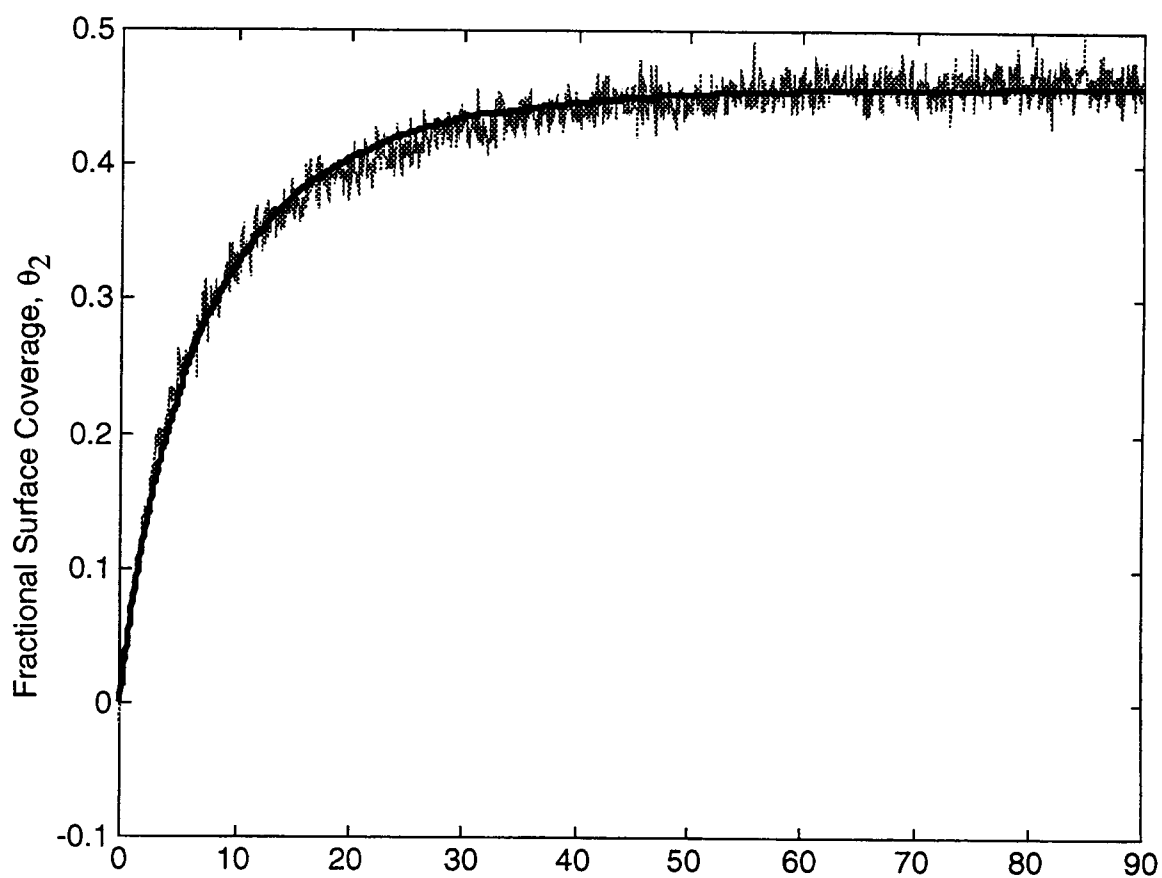


Fig. 4.15. Fractional surface coverage of tryptophan mutant on silica nanoparticles (1:2 mixture). The smooth line is the regressed fit of $\theta_2=f(t)$. ($\Gamma_{\max} = 0.1 \text{ mg}/1.638 \text{ m}^2$)

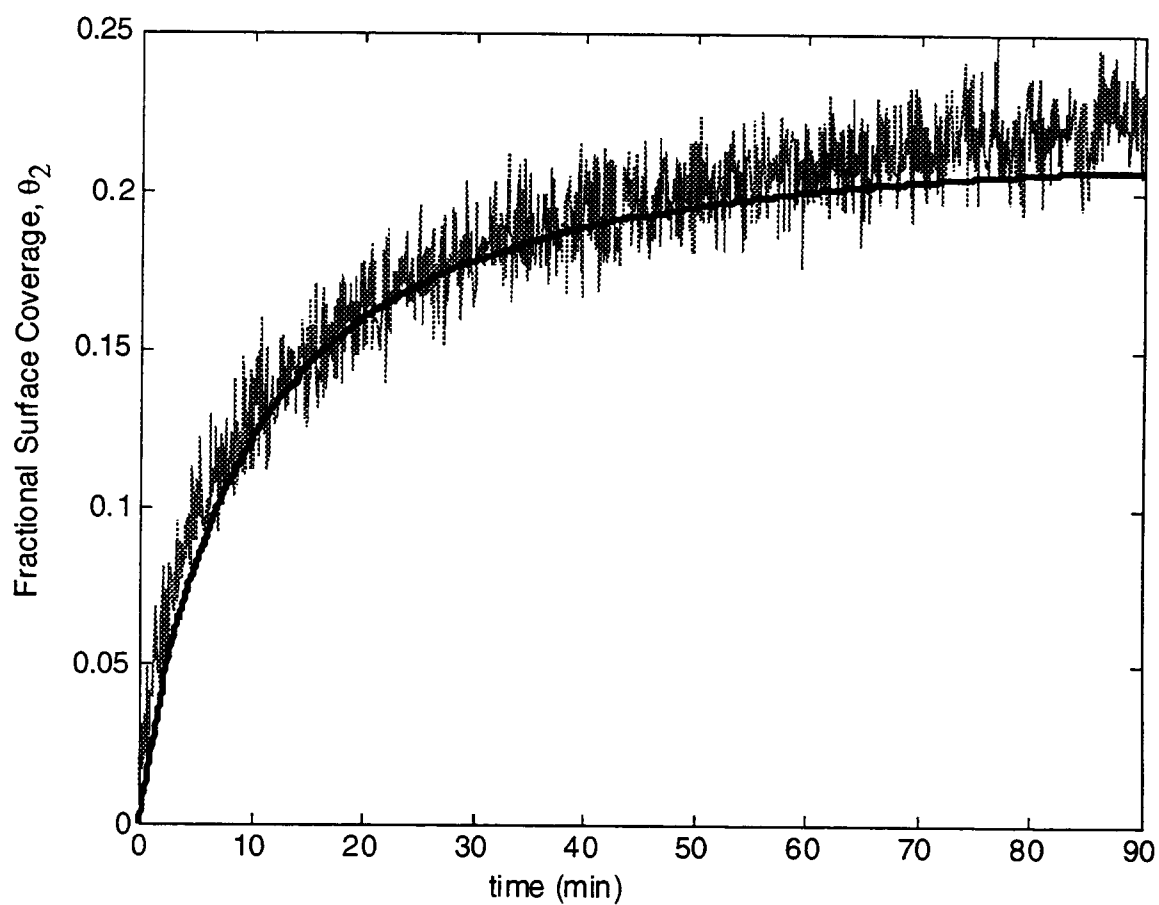


Fig. 4.16. Fractional surface coverage of cysteine mutant on silica nanoparticles (1:2 mixture). The smooth line is the regressed fit of $\theta_2=f(t)$. ($\Gamma_{\max} = 0.1 \text{ mg}/1.638 \text{ m}^2$)

According to the mechanism in Figure 4.9, the CD data correspond to θ_2 , while the ellipsometry kinetic data correspond to total fractional surface coverage ($\theta_1 + \theta_2$). The fit of CD data to the model yielded results for the rate constants of each variant. These rate constants in Table 4.4 were used in the model (equations 4.3 and 4.4) to predict the adsorption kinetics $(\theta_1 + \theta_2) * \Gamma_{\max}$ for the ellipsometry experiments for each variant with the assumption that surface properties in both experiments were comparable. These predictions (presented as total fractional coverage, $\theta_1 + \theta_2$), along with the ellipsometry adsorption kinetic data (presented as total fractional surface coverage, $\theta_1 + \theta_2$) are plotted in Figures 4.18-4.20.

As previously mentioned, in the ellipsometry experiments, monolayer coverage was obtained by all variants except cysteine within the first 30 minutes, multilayer adsorption existed for all variants, and a decrease in adsorbed mass was observed for all variants after buffer rinsing. The plateau value of total fractional surface coverage predicted for the cysteine mutant were higher than that of ellipsometry adsorption kinetic data of this mutant, suggesting that the cysteine mutant did not attain a complete monolayer coverage. The predictions for tryptophan mutant was the best, because the tryptophan mutant had the least multilayer formation, and it is closer to the ideal conditions that described in figure 4.9, that is this model did not take into account of the multilayer formation, and it also did not take into account the interactions between adsorbed molecules. The tryptophan mutant is the least stable mutant, because of its flexibility, the interactions between adsorbed molecules should be the smallest. The prediction for the wild type is almost the best fit for the real experiment curve, the prediction indicated there is some second layer formation.

From the plots, the shapes of the predicted curves (Figures 4.18-4.20) differ to some extent from the shapes of the curves produced from the adsorption kinetic data. In particular, for the first one to two minutes, the adsorbed mass from the ellipsometry

experiments increased faster than the predicted adsorbed mass. After that, the predicted value reached its plateau faster than the ellipsometry kinetic data. This observation is consistent with the hypothesis that an increase in surface coverage could lead to an increase in the energy barrier of adsorption. In other words, the adsorption rates may be functions of surface coverage. A dependence on surface concentration for adsorption rate constants has been proposed by Guzman *et al.* (1986) in terms of activation energies for adsorption and desorption. A first order adsorption rate, represented as $k = k_0 \exp(-E_a/RT)$ where E_a is the activation energy for adsorption, was allowed in that work to increase with surface coverage according to $E_a = E_a^0 + \alpha\Gamma$, where E_a^0 is the activation energy when there is no coverage on the surface, Γ is the fractional surface coverage, and α is a constant. This would require that adsorption rate constants are at their maximum at the beginning of the adsorption, and decrease gradually as the surface coverage increases. Our model assumed that the adsorption rate constants were indeed constant, so the predicted adsorbed mass increased more slowly at first than the experimental data from ellipsometry. The model also predicted that a plateau would be rapidly attained; however this was not observed in the ellipsometry experiments and may be related to multilayer formation. It is not necessary to modify the regression analysis of these CD data according to Guzman *et al.*, since the available surface area was so large that the change in rate constants could be considered negligible. It would probably be necessary to apply such a modification to the analysis of ellipsometry data. So direct application of the rate constants gained from analysis of CD data to the prediction of these adsorption kinetic data is probably sufficient reason for the different shapes between the curves, since CD data were recorded at low surface coverages, while the ellipsometry data were recorded from low to very high surface coverages.

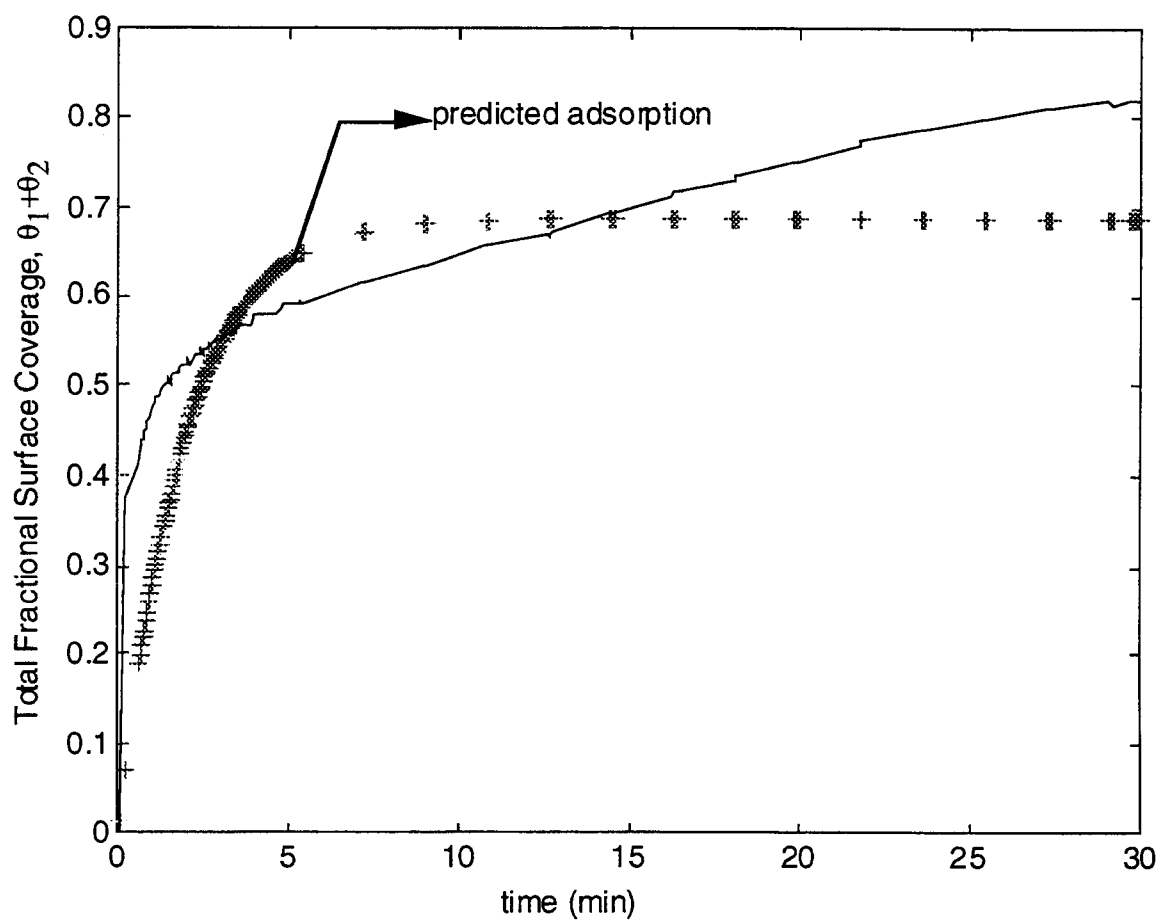


Fig. 4.18. Adsorbed mass (total fractional surface coverage) predicted according to the model by using the rate constants in Table 4.4 for wild type T4 lysozyme along with the empirical ellipsometry adsorption kinetic data.

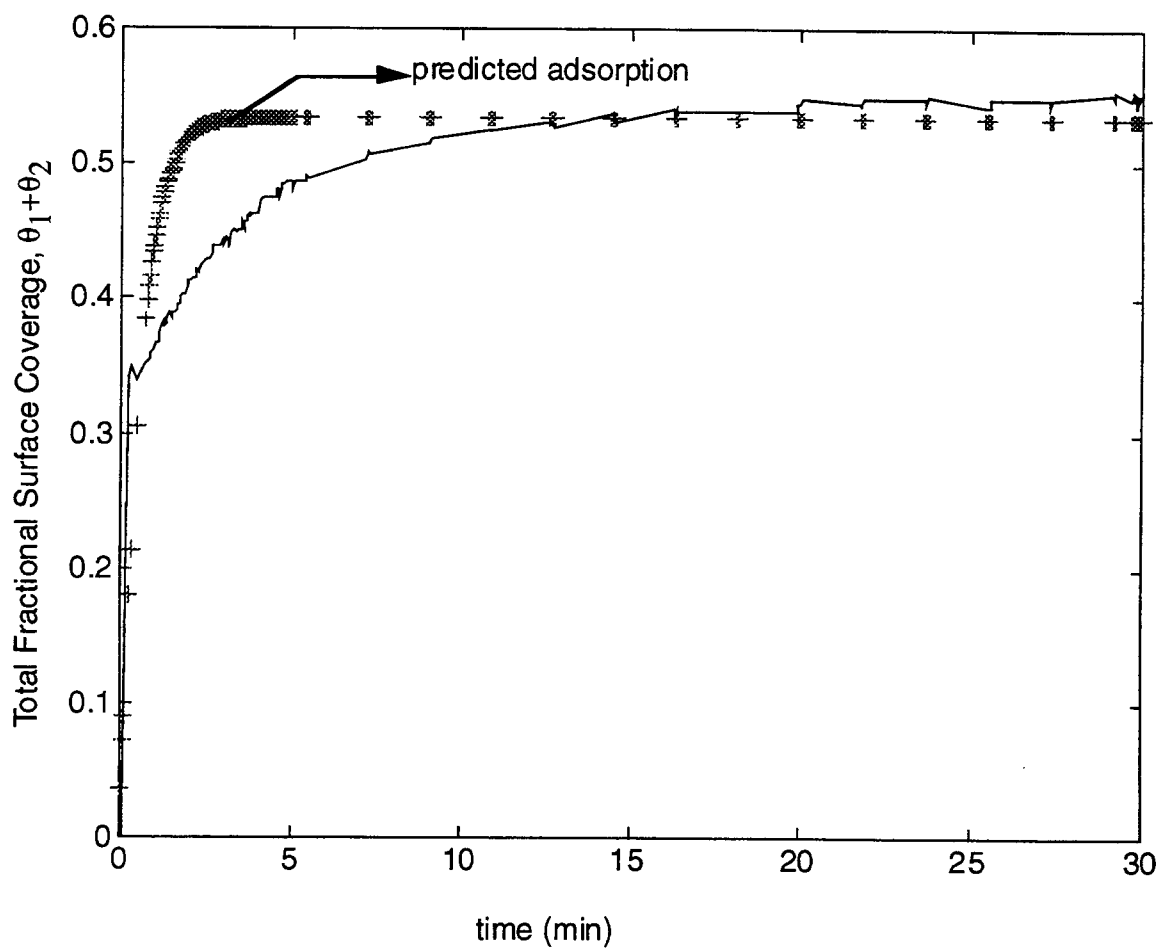


Fig. 4.19. Adsorbed mass (total fractional surface coverage) predicted according to the model by using the rate constants in Table 4.4 for T4 lysozyme tryptophan mutant along with the empirical ellipsometry adsorption kinetic data.

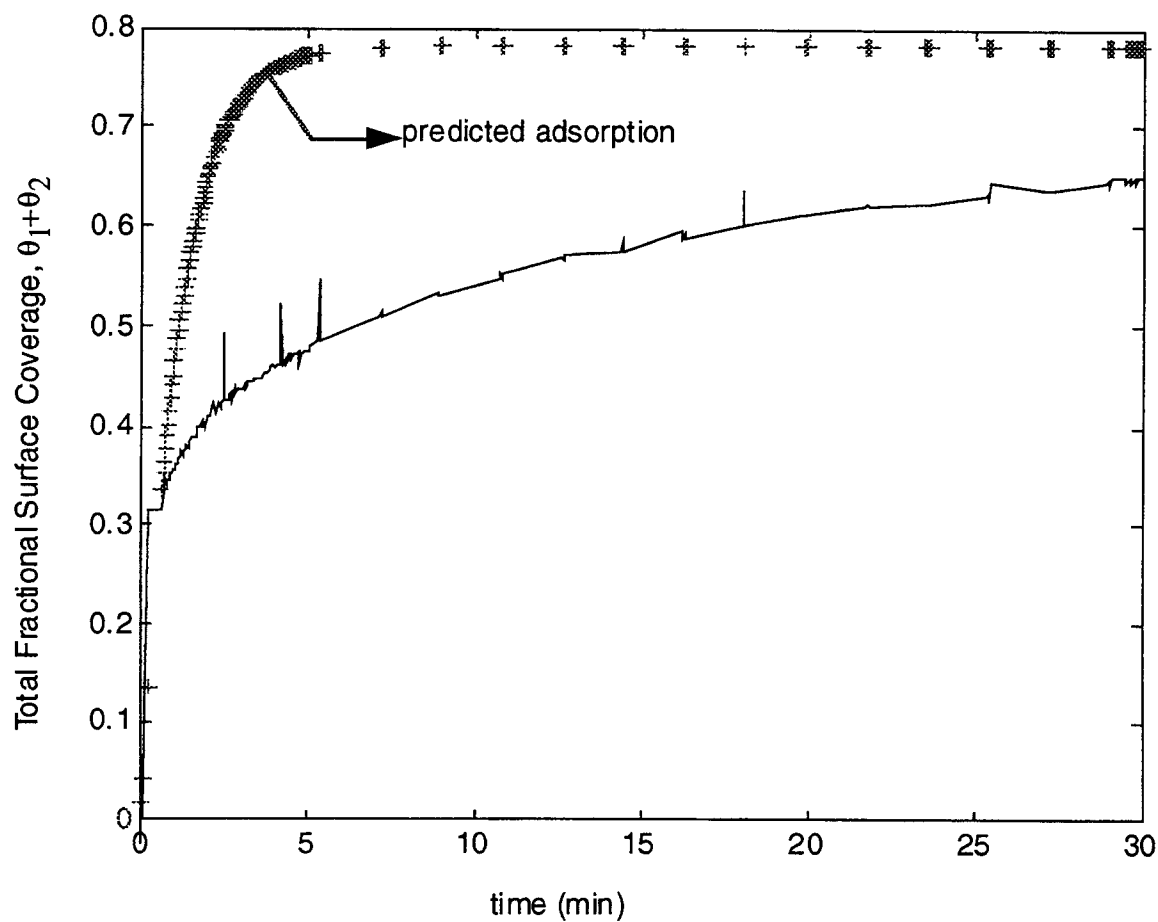


Fig. 4.20. Adsorbed mass (total fractional surface coverage) predicted according to the model by using the rate constants in Table 4.4 for T4 lysozyme cysteine mutant along with the empirical ellipsometry adsorption kinetic data.

4.4 Analysis according to a three-rate-constant adsorption model

Krisdhasima *et al.* (1992), described adsorption kinetics with a mechanism in which irreversible protein adsorption occurs in two steps. In step 1, corresponding to short contact time, the protein molecule reversibly adsorbs to the surface, with its adopted surface conformation closely approximating its native form. In step 2, a surface-induced conformational change takes place, in which the reversibly adsorbed molecule is changed to an irreversibly adsorbed form. The mechanism is illustrated in Figure 4.21.

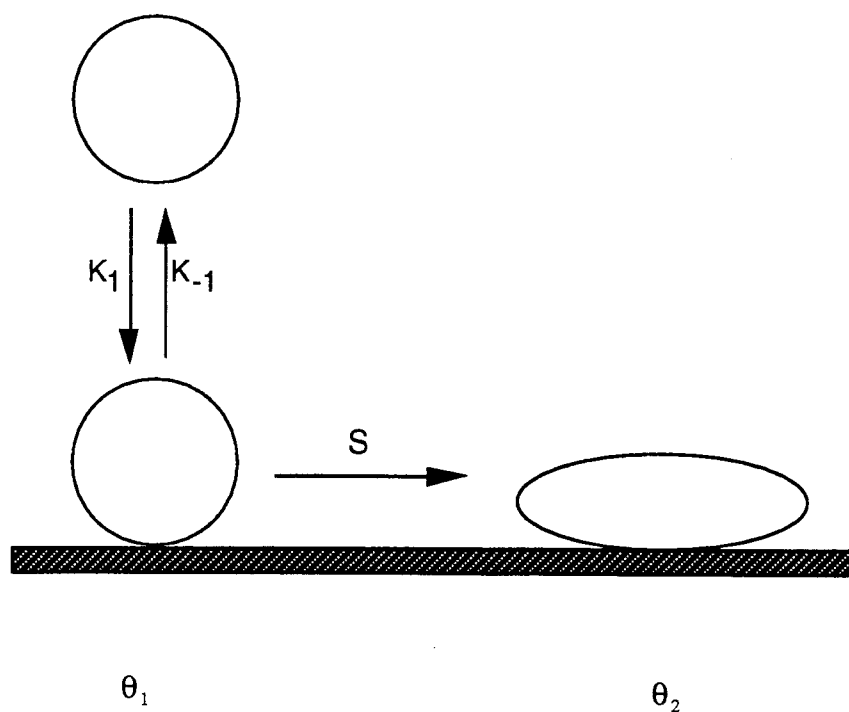


Fig 4.21. A mechanism for T4 lysozyme adsorption into one of two states defined by fractional surface coverages θ_1 and θ_2 , where state 2 molecules occupy a greater surface area than molecules adsorbed in state 1 (Krisdhasima *et al.*, 1992).

The difference between this mechanism and the one shown in Figure 4.9 is that the first one assumes that molecules can adsorb onto the surface directly from the bulk solution, while this one assumes that the conformational change occurs only after molecules have adsorbed in state 1. When ellipsometry data are fit to this model (e.g., Krisdhasima *et al.*, 1992), the fit is quite good, but exact values for the adsorption rate constants can not be determined since there are three unknown variables.

In Figure 4.21, s is defined as the rate of conformational change from state 1 to state 2, k_1 is the rate of adsorption and k_{-1} is the rate of desorption. θ_1 and θ_2 have the same meaning as in Figure 4.9. Equations describing the time-dependent fractional surface coverage of a protein in each of the two states (θ_1 and θ_2) shown in Figure 4.21 can be written as:

$$\frac{d\theta_1}{dt} = k_1 * C * (1 - \theta_1 - a * \theta_2) - k_{-1} * \theta_1 - s * \theta_1 * (1 - \theta_1 - a * \theta_2) \quad [4.10]$$

and

$$\frac{d\theta_2}{dt} = s * \theta_1 * (1 - \theta_1 - a * \theta_2) \quad [4.11]$$

where a and C have the same meaning as in the previous model.

This model contains three unknown variables (k_1 , k_{-1} and s), a simple regression from one kinetic curve is not sufficient to solve for all three values. However, a solution is possible by comparing data from CD and data from ellipsometry (same data used in working with the first model) together to perform the regression. As the ellipsometry data is possibly not appropriate for analysis by a simple one layer model, the emphasis was on CD data during

regression. Because the regressions were performed using the least squares method, the influence of the ellipsometry data during regression was limited by dividing the data by a factor of 30 (the factor 30 was chosen such that the fits of CD data were good enough, while the fits of ellipsometry data were reasonable). Equations [4.10] and [4.11] were applicable to both CD and ellipsometry data, while equation [4.8] was unique to the CD data because it allowed for a concentration change during adsorption. As in the first model, CD data were converted to θ_2 using the equations [4.5] and [4.6]. Equations [4.8], [4.10] and [4.11] were combined together to give the regression for CD data, and equations [4.9] and [4.10] were combined to give the regression for the ellipsometry data.

According to the three-rate-constant model, when $t \rightarrow \infty$, all the molecules adsorbed on the surface will be in state 2. From the plot shown in Figure 4.7, the tryptophan mutant reached an adsorption plateau after 90 minutes, and the cysteine mutant almost reached its adsorption plateau after 90 minutes, although the wild type lysozyme had not yet reached a plateau at this time. We assumed however that all three proteins attained their plateau at 90 minutes, and calculated the percentage of molecules adsorbed at state 2 by equation 4.5, where x is: 29 for tryptophan mutants; 18 for wild type; and 12 for cysteine mutants according to the results in Table 4.2.

The regression along with the data are shown in Figures 4.22-4.24. The adsorption rate constants are tabulated in Table 4.5.

If structural stability is more important in surface-induced unfolding than in initial binding, we would expect similar k_1 and k_{-1} values for all four T4 lysozyme variants, since their three dimensional structures are the same. However, Table 4.5 shows that k_1 and k_{-1} decreased as $\Delta\Delta G^0$ increased. This can be better understood by considering the forces that exist at an interface. Before a protein molecule hits the surface, it encounters an electrical potential barrier for adsorption, and this energy barrier is very significant (Andrade, 1985). It is reasonable to suggest that this interaction between the molecule and the energy barrier

may alter the conformation of the protein to some degree before the protein binds with the surface. This could result in different k_1 and k_{-1} values among the T4 lysozyme mutants.

Table 4.5. Values of the adsorption rate constants estimated with reference to Figure 4.21.

protein	k_1 (ml/mg·min)	k_{-1} (min ⁻¹)	s (min ⁻¹)
Trp mutant	2.02	2.71	0.16
Wild type	1.69	1.10	0.04
Cys mutant	0.40	0.33	0.07

The comparison of Figures 4.10 to 4.22, 4.11 to 4.23, and 4.12 to 4.24 showed that the fit of this model is not as good as the fit to the two-state irreversible adsorption model in a least square sense. The rate constant s , which governs conformational change, would be expected to decrease as the stability of the protein increased; however, from Table 4.5 we can see that this was not the case for wild type and cysteine. The least stable mutant, tryptophan, had the largest value of s , but the most stable mutant, cysteine, did not have the smallest value of s . Possible reasons for this discrepancy include both incomplete coverage of the surface by cysteine mutant molecules and multi-layer formation in the ellipsometry experiments. An overall fit using both ellipsometry and CD data simultaneously would be suspect in any event because the rate constants may depend on the available surface area, and a perfect monolayer coverage is assumed in each case.

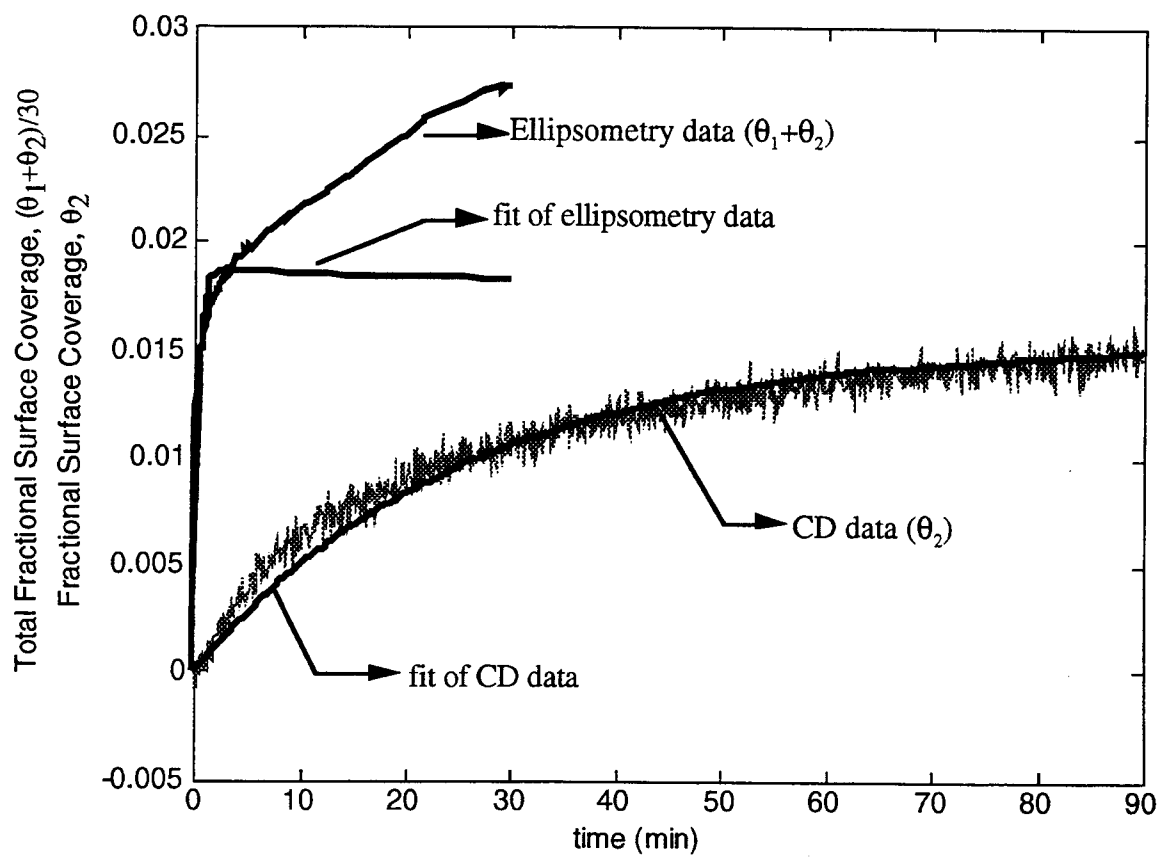


Fig. 4.22. Regression according to the three-rate-constant model for ellipsometry and CD data of wild type T4 lysozyme simultaneously.

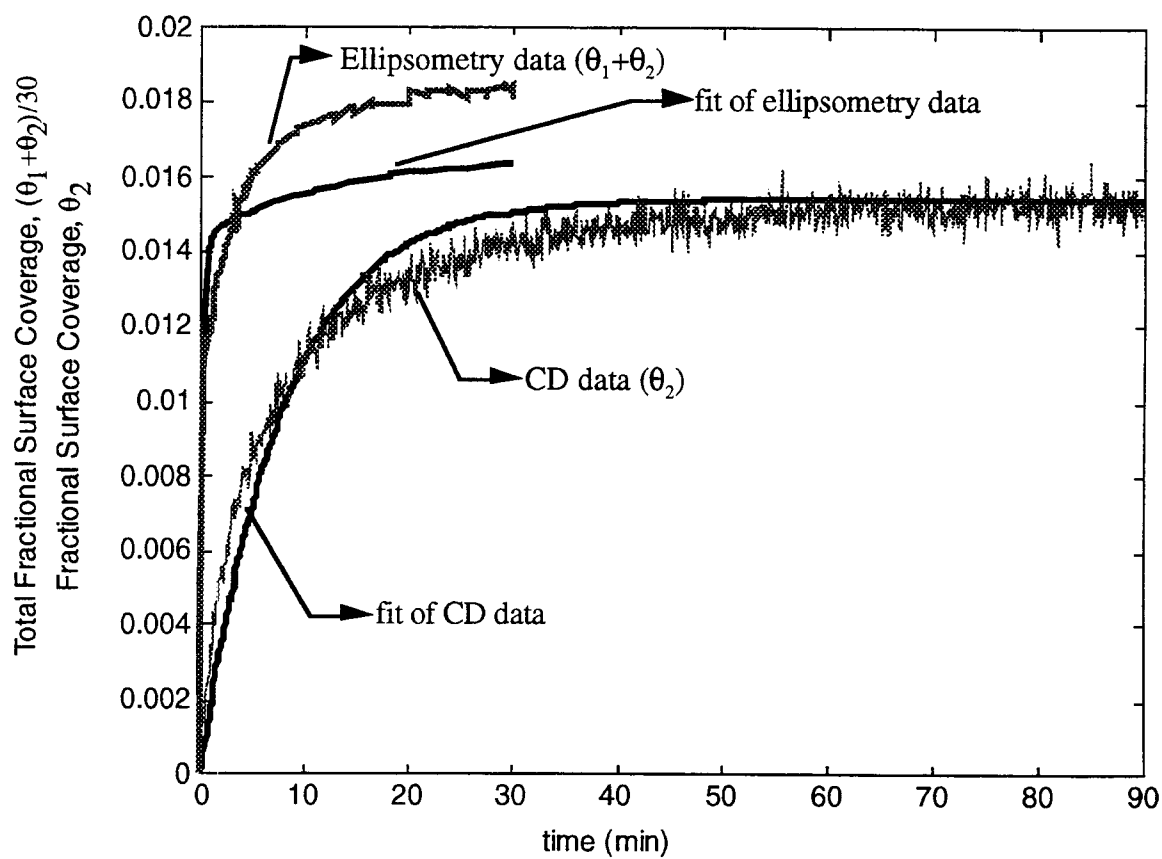


Fig. 4.23. Regression according to the three-rate-constant model for ellipsometry and CD data of T4 lysozyme tryptophan mutant simultaneously.

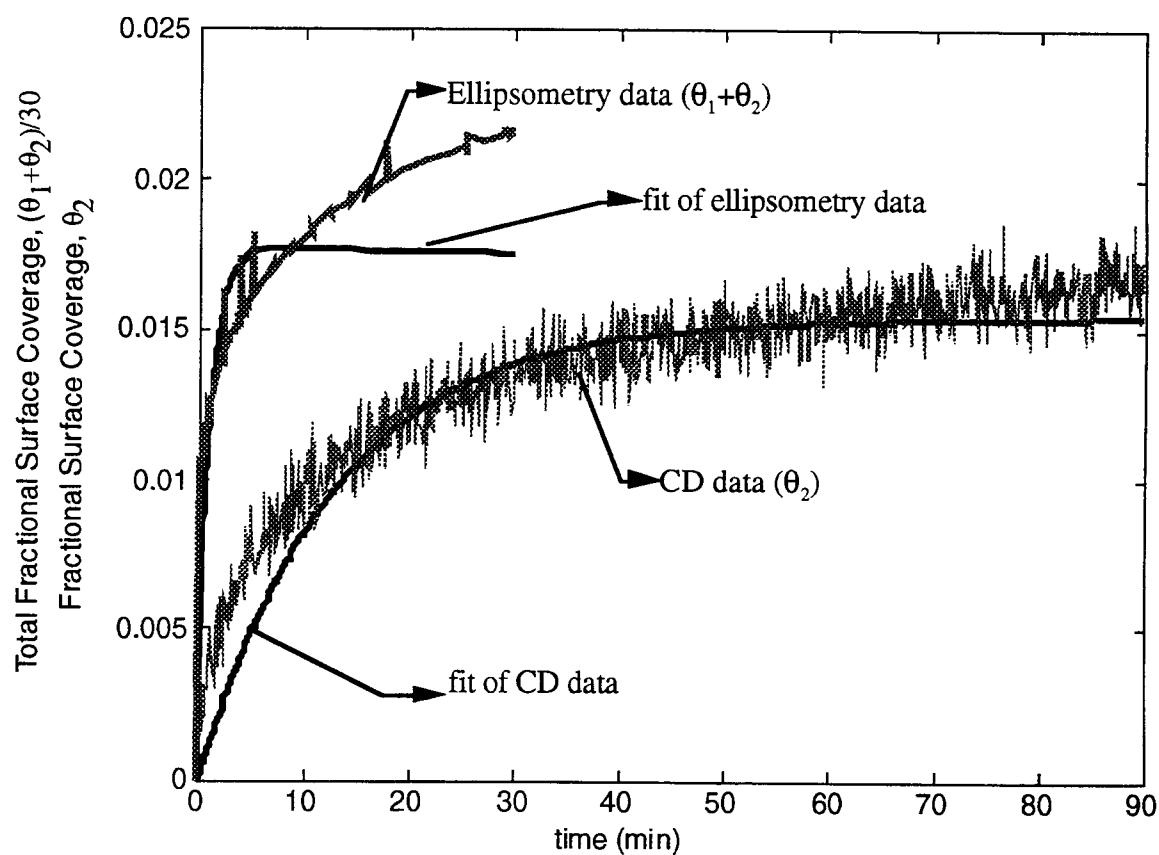


Fig. 4.24. Regression according to the three-rate-constant model for ellipsometry and CD data of T4 lysozyme cysteine mutant simultaneously.

The mechanisms associated with the two models are similar, but the assumptions concerned with the adsorption process for each model are different. The first model assumes that the conformational change of adsorbed proteins happens fast enough to consider the adsorption of state 1 and state 2 molecules occurring simultaneously. The second model assumes that adsorption in state 1 must occur before the molecules undergo a conformational change. In general, the fit of the parallel adsorption model was better than that of the three-rate-constant model. The trends from the rate constants of the parallel adsorption model are what we expected, and it gave reasonable results when it was used to explain ellipsometry adsorption kinetics. Therefore, it is likely that the time required for a molecule to adsorb to a surface is comparable to the time required for conformational change to occur.

CHAPTER 5

CONCLUSIONS

Surface conformational kinetics exhibited by selected stability mutants of bacteriophage T4 lysozyme were measured at the solid-liquid interface using circular dichroism. The data was analyzed with respect to a parallel adsorption model and a three-rate-constant model. The results indicated that protein adsorption at an interface is affected significantly by the conformational stability of protein. The data also suggested that a protein's denaturation upon adsorption at an interface might be a fast event rather than a slow conformational denaturation. The fitting of the data to the models is reasonably good. The first model is more realistic in explaining the data, while both models imply that the rate constants are dependent on the conformational stability of proteins.

BIBLIOGRAPHY

- Alber, T., and Matthews, B. W., The use of x-ray crystallography to determine the relationship between the structure and stability of mutants of Phage T4 lysozyme. *Protein Engineering* (1987)
- Alber, T., and Matthews, B. W., Structure and thermal stability of phage T4 lysozyme, *Methods in enzymology*. **154**:511-533 (1987)
- Anand, K., and Damodaran, S., Kinetics of adsorption of lysozyme and bovine serum albumin at the air-water interface from a binary mixture. *J. Colloid Interface Sci.* **176**:63-73 (1995)
- Andrade, J. D., Principles of protein adsorption ed. Andrade, J. D., *Surface and Interfacial aspects of biomedical polymers* Volume 2 Protein adsorption. Plenum Press Page 1-80 (1985)
- Andrade, J. D., Hlady, V. L., and Van Wagenen, R. A., Effects of Plasma protein adsorption on protein conformation and activity. *Pure & Appl. Chem.* **56**:1345-1350 (1984)
- Beissinger, R. L. and Leonard, E. F., Plasma protein adsorption and desorption rates on quartz: approach to multi-component systems. *Trans. Am. Soc. Artif. Intern. Organs.* **27**:225-230 (1981).
- Billsten, P., Wahlgren, M., Arnebrant, T., McGuire, J., and Elwing, H., Structural changes of T4 lysozyme upon adsorption to silica nanoparticles measured by circular dichroism. *J. Colloid Interface Sci.* **175**:77-82 (1995)
- Brash, J. L., and Horbett, T. A., *Proteins at interface* ed. Brash, J. L., and Horbett, T. A., ACS Press Page 1-23 (1995)
- Brittain, H. G., Introduction to chiroptical phenomena. *Analytical applications of circular dichroism*, ed. N. Purdie and H. G. Brittain, 1-13. ELSEVIER (1994)
- Chen, G. C., and Yang, J. T., Two point calibration of circular dichrometer with d-10-camphorsulfonic acid. *Anal. Lett.* **10**:1195-1207 (1977)
- Clark, S. R., Billsten, P., and Elwing, H., A fluorescence technique for investigating protein adsorption phenomena at a colloidal silica surface. *Colloids and interfaces B: Biointerfaces*, **2**:457-461 (1994)
- Drake, A. F., Circular dichroism. ed. Jones, C., and Thomas, A. H., *Method in molecular biology* **22**:219-245 (1994)
- Elwing, H., Nilsson, B., Svensson, K., Askendahl, A., Nilsson, U., and Lundström, I., Conformational changes of a model protein (complement factor 3) adsorbed on hydrophilic and hydrophobic solid surfaces. *J. Colloid Interface Sci.* **125**:139-145 (1988)
- Guzman, R. Z., Carbonell, R. G., and Kilpatrick, P. K., The adsorption of proteins to gas-liquid interfaces. *J. Colloid Interface Sci.* **114**:536-547 (1986)

- Haynes, C. A., and Norde, W., Structures and stabilities of adsorbed proteins. *J. Colloid Interface Sci.* **169**:313-328 (1995)
- Hlady, V., and Andrade, J. D., Fluorescence emission from adsorbed bovine serum albumin and albumin-bound 1-anilinonaphthalene-8-sulfonate studied by TIRF. *Colloids and surfaces* **32**:359-369 (1988)
- Horbett, T. A., and Brash, J. L., *Proteins at interfaces: current issues and future prospects*. ed. Brash, J. L., and Horbett, T. A., ACS press Page 1-33 (1987)
- Hunter, R. J., *Introduction to modern colloid science*, Oxford university press, Page 32-56 (1993)
- Johnson, W. C., Circular dichroism and its empirical application to biopolymers, *Methods of biochemical analysis* **31**:61-115 (1985)
- Johnson, W. C., Protein secondary structure and circular dichroism: a practical guide. *Proteins: Structure, Function, and Genetics* **7**:205-214 (1990)
- Johnson, W. C., Circular dichroism instrumentation, *Circular dichroism and the conformational analysis of biomolecules*, edited by Gerald D. Fasman. Plenum Press, New York (1996)
- Kato, K., Sano, S., and Ikada, Y., Protein adsorption onto ionic surfaces. *Colloids and surfaces B: biointerfaces* **4**:221-230 (1995)
- Kondo, A., and Higashitani, K., Adsorption of model proteins with wide variation in molecular properties on colloidal particles. *J. Colloid Interface Sci.* **150**:344-351 (1992)
- Kondo, A., Oku, S., and Higashitani, K., Structural changes in protein molecules adsorbed on ultrafine silica particles. *J. Colloid Interface Sci.* **143**:214-221 (1991)
- Kondo, A., Murakami, F., and Higashitani, K., Circular dichroism studies on conformational changes in protein molecules upon adsorption on ultrafine polystyrene particles. *Biotechnology and Bioengineering* **40**:889-894 (1992)
- Krisdhasima, V., McGuire, J., and Sproull, R., Surface hydrophobic influence on β -lactoglobulin adsorption kinetic. *J. Colloid Interface Sci.* **154**:337-350 (1992)
- Lu, D., and Park, K., Effect of surface hydrophobicity on the conformational changes of adsorbed fibrinogen. *J. Colloid Interface Sci.* **144**:271-281 (1991)
- Lundström, I., Models of protein adsorption on solid surfaces. *Prog Colloid & Polymer Sci.* **70**:76-82 (1985).
- Lundström, I., and Elwing, H., Simple kinetic models for protein exchange reactions on solid surfaces. *J. Colloid Interface Sci.* **136**:68-84 (1990).
- Malmsten, M., Ellipsometry studies of the effects of surface hydrophobicity on protein adsorption. *Colloids and surfaces B: Biointerfaces* **3**:297-308 (1995).
- Matthews, B. W., Dahlquist, F. W., and Maynard, A. Y., Crystallographic data for lysozyme from bacteriophage T4. *J. Mol. Biol.* **78**:575 (1973)

- Matsumura, M., Becktel, W. J., and Matthews, B. W., Hydrophobic stabilization in T4 lysozyme determined directly by multiple substitutions of Ile 3. *Nature* 334:406-410 (1988)
- McGuire, J., Wahlgren, M. C., and Arnebrant, T., Structural stability effects on the adsorption and dodecyltrimethylammonium bromide-mediated elutability of bacteriophage T4 lysozyme at silica surfaces. *J. Colloid Interface Sci.* 170:182-192 (1995).
- Mizutani, T. J., Decreased activity of protein adsorbed onto glass surfaces with porous glass as a reference. *J. Pharm. Sci.* 69:279-281 (1980)
- Norde, W., Macritchie, F., Nowicka, G., and Lyklema, J., Protein adsorption at solid-liquid interfaces: reversibility and conformation aspects. *J. Colloid Interface Sci.* 112:447-456 (1986)
- Pitt, W. G., Fabrizio-Homan, D. J., Mosher, D. F., and Cooper, S. L., Vitronectin adsorption on polystyrene and oxidized polystyrene. *J. Colloid Interface Sci.* 129:231-239 (1989)
- Ramsden, J. J., and Prenosil, J. E., Effects of ionic strength on protein adsorption kinetics. *J. Phys. Chem.* 98:5376-5381 (1994)
- Sadana, A., Protein adsorption and inactivation on surfaces. influence of heterogeneities. *Chem. Rev.* 92:1799-1818 (1992)
- Shirahama, H., Lyklema, J., and Norde, W., Comparative protein adsorption in model system. *J. Colloid Interface Sci.* 139:177-187 (1990)
- Smith, L. J., and Clark, D. C., Measurement of the secondary structure of adsorbed protein by circular dichroism. 1. Measurement of the helix content of adsorbed melittin. *Biochimica et biophysica acta* 1121:111-118 (1992)
- Snatzke, G., Circular dichroism: an introduction. *Circular dichroism principles and applications*, ed. K. Nakanishi, N. Berova, and R. W. Woody, 1-38. VCH (1994).
- Soderquist, M. E., and Walton, A. G., Structural changes in proteins adsorbed on polymer surfaces. *J. Colloid Interface Sci.* 75:386-397 (1980)
- Sun, D., Söderlind, E., Baase, W. A., Wozniak, J. A., Sauer, U., and Matthews, B. W., Cumulative site-directed charge-change replacements in bacteriophage T4 lysozyme suggest that long-range electrostatic interactions contribute little to protein stability. *J. Mol. Biol.* 221:873-887(1991)
- Tan, J. S., and Martic, P. A., Protein adsorption and conformational change on small polymer particles. *J. Colloid Interface Sci.* 136:415-431 (1990)
- Toumadje, A., Alcorn, S. W., and Johnson, W. C., Extending CD spectra of proteins to 168 nm improves the analysis for secondary structures. *Analytical biochemistry* 200:321-331 (1992)
- Wang, Jun Surface tension kinetics of the wild type and four synthetic structural stability mutants of bacteriophage T4 lysozyme at the air-water interface Valley library, OSU (1995)

Weaver, L. H., and Matthews, B. W., Structural of bacteriophage T4 lysozyme refined at 1.7 Å resolution. *J. Mol. Biol.* **193**:189-199 (1987)

Wozniak, J. A., Zhang, X.-J., Weaver, L. H., and Matthews, B. W., Structural and genetic analysis of the stability and function of T4 lysozyme, ed. Jim D. Karam, *Molecular biology of bacteriophage T4*. 332-339. ASM Press (1994)

Zhong, L., and Johnson, W. C. Jr, Environment affects amino acid preference for secondary structure. *Proc. Natl. Acad. Sci.* **89**:4462-4465 (1992)